General Disclaimer

One or more of the Following Statements may affect this Document

- This document has been reproduced from the best copy furnished by the organizational source. It is being released in the interest of making available as much information as possible.

- This document may contain data, which exceeds the sheet parameters. It was furnished in this condition by the organizational source and is the best copy available.

- This document may contain tone-on-tone or color graphs, charts and/or pictures, which have been reproduced in black and white.

- This document is paginated as submitted by the original source.

- Portions of this document are not fully legible due to the historical nature of some of the material. However, it is the best reproduction available from the original submission.

Produced by the NASA Center for Aerospace Information (CASI)

NASA CONTRACTOR REPORT 166593

(NASA-CR-166593) IN-SITU TEM INVESTIGATIONS OF GRAPHIC-EPITAXY AND SMALL PARTICLES Final Report, 1 Jan. - 31 Dec. 1982 (Eloret Corp.) 68 p HC A04/MF A01 CSCL 20L

N84-32201

Unclas
G3/76 00813

In-Situ TEM Investigations of Grapho-Epitaxy and Small Particles

K. Heinemann

CONTRACT NCC2-171
January 1983

NASA

NASA CONTRACTOR REPORT 166593

In-Situ TEM Investigations of Grapho-Epitaxy and Small Particles

K. Heinemann

Cooperative Agreement NCC2-171

National Aeronautics and
Space Administration

Ames Research Center
Moffett Field, California 94035

ABSTRACT

Palladium was deposited inside a controlled-vacuum specimen chamber of a transmission electron microscope (TEM) onto freshly prepared MgO and α-alumina substrate surfaces. Annealing and various effects of gas exposure of the particulate Pd deposits were studied in-situ by high-resolution TEM and electron diffraction. Whereas substrate temperatures of 500 C or annealing of room-temperature (RT) deposits to 500 C were needed to obtain epitaxy on sapphire, RT-deposits on MgO were perfectly epitaxial. For Pd/MgO a lattice expansion of 2-4% was noted; the highest values of expansion (compared to the bulk Pd lattice parameter) were found for the smallest particles. The lattice expansion of small Pd particles on alumina substrates was less than 1%. Long-time RT exposure of Pd/MgO in a vacuum of 10^{-8} millibar (major residual gas components were water and CO) yielded some mobility and coalescence events, but notably fewer than for Pd on sapphire. Exposure to laboratory air or oxygen greatly enhanced the particle mobility and coalescence and also resulted in the flattening of Pd particles on MgO substrates. Electron-beam irradiation further enhanced this effect. Exposure to laboratory air for several tens of hours of Pd/MgO led to strong coalescence with a tendency of minimization of the particle surface areas by promoting 3-dimensional Pd particle habit formation. The observations were explained in terms of strong metal/ support interactions of Pd/MgO. The results also indicate

that small deposited metal particles may undergo appreciable changes when exposed to air at RT, such as is common practice in ex-situ TEM investigations of particulate deposits.

INTRODUCTION

ORIGINAL PAGE IS
OF POOR QUALITY

Progress of modern catalysis research has spurred a renewed interest in small-particle research. The determination of the crystal structure and habit planes of nanometer-size particles has mostly been reserved to various TEM approaches. In the vast majority of all such work reported, the particles were prepared (i) outside the vacuum system in which they were subsequently investigated, and (ii) often many hours or days before the TEM studies actually started, and little if any attention has been directed to the influence that this treatment of the deposit prior to the TEM studies might have had on the results. In the present work we have employed the in-situ TEM technique, where the depositions and subsequent TEM analysis are performed in the TEM under controlled vacuum conditions (1), for the study of this effect.

As important as controlled vacuum conditions -- achieved in our in-situ approach by replacing the regular TEM specimen chamber with a uhv-compatible advanced custom chamber that is differentially pumped -- is the availability of clean substrates for such work. Single crystal thin, electron transparent films of MgO (2,3) and sapphire (4-6) can be produced by in-situ electron-beam flash heating of chemically pre-thinned MgO disks and amorphous alumina

films, respectively. Since the cleanliness of these two types of substrates has been well documented, and since MgO and alumina are substrates of interest in catalysis -- the former being representative of strong, the latter of weak metal/substrate interaction -- we have chosen MgO and alumina as substrates for this work.

With an in-situ TEM facility that allows operation under controlled vacuum conditions at high image resolution we have studied the nucleation and early growth of Pd from the vapor phase, the respective epitaxy and pseudo-morphism, and the exposures to various gases of palladium on MgO and alumina substrate surfaces at various temperatures.

ORIGINAL PAGE IS
OF POOR QUALITY

EXPERIMENTAL

Palladium was evaporated from an electron-beam heated source installed in a custom stainless steel specimen chamber fitted to a Siemens Elmiskop 101 transmission electron microscope (TEM) converted for in-situ experimentation (6). The evaporation rate and deposit thickness were monitored with a quartz crystal micro-balance. A rate of 3×10^{13} atoms/cm^2/sec was maintained for all depositions. The maximum average deposit thickness was 1.8 nm, if unity sticking probability on the quartz crystal is assumed. The chamber, evacuated with a helium cryopump, was at a pressure in the mid 10^{-9} millibar range (1 millibar = 0.75 torr) before and after the depositions. The chamber pressure increased by approximately one order of magnitude during the depositions.

In order to minimize the influence of the imaging electron beam, its intensity was maintained below 0.1 A/cm^2, and the total beam exposure of the specimen areas of interest was minimized (to below a few tens of A sec/cm^2 -- 1 Asec/cm^2 = 6242 electrons/nm) by performing all routine TEM image adjustments at specimen regions outside those of interest, except for those experiments where specimen irradiation damage itself was the object of the investigation.

The alumina substrates were prepared by anodic oxidation at 45 V of 0.025 mm thick aluminum foil and by subsequent

dissolution of the unoxidized aluminum in a saturated HgCl2 solution. The resulting approximately 100 nm thick amorphous alumina films were washed in distilled water, transferred to a specimen grid, and mounted in the specimen stage of the TEM. Clean, single crystal sapphire substrate areas of various orientations were obtained by electron-beam flash heating immediately prior to the deposition (5,6,7).

Magnesium-oxide substrates were prepared from 0,5 mm thick MgO disks of 3 mm diameter by chemical pre-thinning with hot, concentrated phosphoric acid in a dual-Jet TEM specimen thinning apparatus until a hole formed in the center of the disk. The pre-thinned specimen was then washed carefully in methanol and inserted in the hot stage of the TEM. Clean, electron-transparent areas of MgO in {100} and {111} orientation were obtained by electron- beam flash heating immediately prior to beginning the deposition (2).

The experimental conditions for the preparation of clean substrate areas by electron-beam flash heating were the same for both types of specimens and were essentially independent of the substrate temperature: exposure of a selected specimen area (near the edge of the hole in the case of MgO) with a beam of approximately 15 microns in diameter at 2-8 A/cm2 intensity for a fraction of a second,

regulated by passing with the final condenser lens through focus, produced the required single crystal specimen regions (3,5,7). The preparation of clean, electron-transparent specimen areas by flash heating could be repeated several times for subsequent deposition experiments. The high momentary temperature conditions associated with this technique cause any deposits, including previous palladium islands and hydrocarbon contaminants, should they be present, to evaporate (6), thus leaving clean substrate surfaces regardless of the deposition history of the sample.

The depositions on MgO surfaces were performed at room temperature (RT) or at slightly elevated temperature. The substrate temperatures for depositions on alumina varied between RT and 700 C. In order to be able to quickly reach the temperature equilibrium necessary for high-resolution microscopy, the work on alumina substrates was done with a direct-grid heater hot stage (6,8), whereas the MgO disks had to be mounted in a more conventional, indirectly heated hot stage. The grid-heater stage had the added advantage of maintaining the TEM manufacturer- recommended vertical (z-) position of the specimen in the objective lens, thus operating under optimum focal length and lens aberration conditions. The vacuum seal between the custom deposition/specimen chamber and the TEM objective lens required the specimen position to be raised by

approximately 1 mm in the case of the conventional, indirectly heated hot stage. However, we found that the sacrifice in image resolution due to this increase in spherical and chromatic aberration constants was hardly noticeable. We were able to clearly image palladium clusters below 1 nm in diameter with both types of stages.

A typical experimental sequence consisted of (a) preparation of a clean, single crystal specimen area, (b) evaporation of palladium (usually with the imaging electron beam off), and (c) the generation of a defocus series of high resolution TEM images and of a few selected-area diffraction (SAD) patterns. Step (c) was sometimes repeated after various time intervals of uhv annealing, or after admitting gases (oxygen or hydrogen at low pressures, typically for several hundred Langmuirs) or laboratory air (at atmospheric pressure).

In a few cases, a specimen was transferred to a high-resolution Hitachi H-500H TEM for extended-period air exposure and selected-zone dark field (SZDF) work (9).

The resulting electron micrographs were evaluated in terms of palladium island number density, surface coverage, and size distribution with a Zeiss Videomat image analyzer.

RESULTS

ORIGINAL PAGE IS
OF POOR QUALITY

1. PALLADIUM ON SAPPHIRE

Epitaxy and Gas Exposures

Depositions at room temperature yielded very small crystals at very high number density, quite ramdomly oriented (only exhibiting a very slight texture), as is shown in the micrograph and the diffraction pattern of Fig. 1 for the case of a nominal 0.6 nm thick deposit. Raising the substrate temperature to 600 C produced much larger, epitaxially oriented particles (Fig.2). Practically the same result in terms of average particle size, number density, and epitaxial orientation can be obtained by short duration annealing of an RT-deposit, as is shown in Fig.3b, where the specimen of Fig. 3a with a 0.2 nm RT-deposit was heated for 3 min at 500 C at a total pressure of 2×10^{-8} millibar. Fig. 3c and d give an example of the effect of subsequent exposure to oxygen and hydrogen (each for 10 min at 1×10^{-5} millibar and 200 C), respectively. Whereas a significant number of cluster mobility and coalescence events has taken place during the oxygen annealing (Fig.3c), further changes during subsequent hydrogen annealing were not noted (Fig.3d). The latter is expected sice hydrogen desorbs from Pd at temperatures as low as 100 C. The changes during oxygen annealing include also structural rearrangements, evidenced in an increase of Pd

ORIGINAL P.
OF POOR QU.

200 and a strong decrease of Pd 111 diffraction intensities in Fig. 3c.

Lattice Expansion

Measurements of the lattice parameter of the palladium overgrowth, using the alumina reflections as internal standard, yielded a value about 0.75% larger than bulk palladium. However, such measurements are difficult and might at times be doubtful if the substrate is not perfectly planar within the selected area. For example, the bending of the alumina substrate in Fig. 3 caused apparent changes of the d-spacings of the respective alumina planes by as much as 1%, thus invalidating the use of these diffraction patterns as reliable standards. However, the diffraction pattern of Fig.2 shows a low degree of such distortion; the above value of 0.75% was averaged from this and similar diffraction patterns.

With a somewhat lesser degree of confidence we determined that the lattice parameter of the palladium islands expanded to a total of about 2% (+-1%) upon annealing in oxygen at 200 C, such as done between Figs. 3b and 3c. Further annealing in hydrogen (Fig. 3d) did not affect the lattice parameter of the Pd island deposit.

2. PALLADIUM ON MgO

Nucleation and Epitaxy

As known from our previous work, the MgO substrate preparation method by electron-beam flash heating produces two types of substrate orientations, {100} and {111} . Since {100} surfaces were produced much more frequently, and since there were no indications that the major results were dependent on the orientation of the substrate surface, we are reporting here mostly results obtained on {100} MgO.

A sequence of images of typical RT-deposits of 0.3, 0.6, 1.2, and 1.8 nm nominal thickness on {100} MgO is shown in Fig.4. The number density of the palladium islands, the area coverage, and the average particle size are plotted in Figs.5-7. Whereas the determination of area coverages with an image analyzer working on the principle of gray level discrimination is quite reliable, the measurement of mean particle sizes or size distributions can be quite ambiguous for small particles, since the gray-level contrast of such particles depends strongly on the TEM focus condition and on background intensity variations. We have, therefore,

relied on a calculation rather than a measurement of the mean particle diameter (Dm). If Θ is the measured area coverage ($0 < \Theta < 1$), if N is the measured particle number per cm^2, and if we assume circular particle projections and hemispherical particle shapes, we get

$$\Theta = 10^{-14} N \pi \frac{D^2}{4} \qquad (1)$$

and therefore

$$D = 1.13 \times 10^{7} \left(\Theta/N\right)^{1/2} \qquad (2)$$

A typical deposition - annealing sequence (all at RT) is presented in Fig.8, showing in (a) the as-"cleaved" MgO substrate, in (b) the 0.3 nm Pd deposit shortly after deposition, and in (c) the same deposit after 21 hours annealing. Careful examination of the figure indicates that some coalescence events and mobility events (one example each is shown in the circle and the square, respectively) occurred under these RT high vacuum (2×10^{-8} millibar) annealing conditions. The effect of high vacuum, low- temperature annealing decreases with increased average deposit thickness. For twice the deposit thickness, much fewer coalescence events were found, and practically no annealing effect was noted for a 1.2 nm deposit as shown in Fig.9.

ORIGINAL PAGE IS
OF POOR QUALITY

Lattice Expansion

Whereas deposits of palladium on sapphire substrates showed clear Pd diffraction intensities in SAD patterns even for thin deposits (e.g., Fig. 3 which represents a 0.2 nm deposit), the detection of diffraction intensities for Pd on MgO was considerably more difficult. Fourfold thicker deposits were the approximate lower detection limit. But even for this deposit thickness the Pd diffraction spots were so weak that the photoplates had to be intentionally overexposed, and the results had to be compared with those of substantially heavier deposits, such as 1.2 or 1.8 nm, in order to make reliable measurements. In Fig. 10 we present as example two diffraction patterns representative of 1.2 nm and 1.8 nm deposits on {100} MgO. Apart from the fact that Fig. 10 indicates near-to perfect epitaxy for these RT deposits, one can notice that the Pd diffraction spots are relatively broad, and measurements of the spot spacings, using the perfect MgO 200 and 220 type spots as internal standard, indicate that the corresponding lattice parameter is substantially larger than that of bulk palladium. Measurements using results from several diffraction patterns and from several depositions for each thickness indicate that this "lattice expansion" amounts to 2.5 - 3% for deposits thicker than 0.9 nm (average), and that it increases notably for thinner

deposits. No changes in the diffraction patterns were observed upon RT annealing or exposure of the deposits to gases or laboratory air. It should be noted, however, that our experiments do not allow any conclusion about the question whether the entire unit cell is expanded, or if the expansion observed in the direction parallel to the substrate surface is concomitant with less expansion or even contraction in the direction normal to the substrate surface, thus reducing the unit cell volume increase. Information about lattice expansion on {111} MgO was not obtained because of difficulties in the measurement of MgO d-spacings which are subject to changes due to strong bending and concomitant diffraction contrast changes within even small selected areas.

Gas Exposures

Exposure of Pd/MgO deposits to oxygen or air at RT yielded marked changes beyond those that are obtained during RT vacuum annealing alone. An example for a 0.3 nm deposit is presented in Fig. 11, showing the condition 7 min after deposition in (a), and the conditions 2.5 min, 36 min, and 200 min following oxygen exposure at 2×10^{-6} millibar for 3 min in (b), (c), and (d), respectively. The circles in (b) indicate some of the many coalescence events that have occurred due to the oxygen exposure. The triangle denotes

a particle that has changed into a distinct, triangular shape. Further mobility during additional annealing was then relatively infrequent. This result indicates that due to the oxygen exposure we observe particle mobility and coalescence as in the case vacuum annealing, but that the relative number of events is markedly increased.

Even more significant changes are observed if thin Pd/MgO deposits are exposed for short durations to laboratory air at atmospheric pressure, as is demonstrated in Fig.12 for the case of a typical 0.9 nm deposit. The particle number density has decreased by 16%, and the decoration of substrate surface steps seems to have become more pronounced (see arrow). In Fig.13 we present an example of a thicker RT-deposit (1.8 nm) that had been exposed to air three times, once for 10 min while still in the specimen stage of the in-situ TEM facility (Fig.13b), once for some 30 min during transfer to the Hitachi H500H high-resolution microscope (Fig.13c), and once for 120 hours in a long-term laboratory air exposure experiment (Fig.13d). One can see that the particles have moved toward each other, often forming chains of particles that have coalesced but not yet sintered into new, homogeneous single crystal, hemispherical particles. The changes are most pronounced between the as-deposited stage (Fig.13a) and the first air exposure (Fig.13b), and the process continued during the second air exposure at a slower rate. However, the changes

due to exposure to laboratory air apparently continue to occur for long times. Fig. 13d reveals a substantial additional change after 120 hours of air exposure. Whereas the previous particle shapes had predominantly been square or rectangular, most facets seemed to have disappeared during the prolonged air exposure, leaving chains of particles with essentially round profiles. But even in this progressed stage of coalescence -- there is also a significant number of additional coalescence events in Fig.13d when compared to Fig.13c -- complete sintering into new, homogeneous single crystal particles has not occurred. This is demonstrated in the micrograph of Fig.14, which was taken after Fig.13d. Fig.14 shows one bright field and two SZDF exposures, imaged with the Pd 200 zone; Fig. 14b is in focussed condition and Fig.14c is a double exposure of two defocussed conditions. These micrographs illustrate (see circled area) that the Pd diffraction intensities still stem from the original, then separated crystallites. Fig.14c also indicates that the <001> direction in the deposit is at an unexpected 45 degree angle with respect to substrate surface steps.

The long-term annealing effect was quite different if the annealing, following a few minutes of exposure to laboratory air at atmospheric pressure, was performed in vacuo (1×10^{-8} millibar). This can be seen in Fig.15 for the case of a 0.3 nm Pd deposit on MgO before and after such treatment; significant spreading of some of the Pd particles occurred on the {111} substrate area (see circled area as an example) and almost complete spreading, leading essentially to disappearance of most of the Pd particles, was observed in the {100} MgO areas (top of Fig.15).

Electron-Beam Induced Effects

Fig.16 demonstrates the typical influence of the electron beam. During the electron microscopy leading to Fig.16c, a total beam exposure of 180 A sec/cm2 was logged. The irradiation was then intentially prolonged by another 150 A sec/cm2 at a slightly increased rate, leading to Fig.16d. A twofold effect is noticed: First, a build-up of material, similar to the common hydrocarbon contamination has occurred as can be seen along the edge of the MgO substrate area. However, particle mobility was not suppressed as expected from a hydrocarbon contamination "fixing" layer. Second, strong phase contrast features appear along the left hand side of the selected micrograph area, concomitant with a decrease of contrast and/or

complete disappearance of the Pd particles. More careful examination of micrographs of this kind revealed that this effect is enhanced with increasing specimen thickness, as would be expected from radiation damage in the bulk of the MgO support.

We observed a significant enhancement of the radiation damage effect when the specimen had also been exposed to laboratory air at atmospheric pressure (inside the EM specimen stage for a few minutes). Fig. 17 shows a 0.3 nm Pd deposit on {111} MgO after deposition (Fig.17a) and 100 hours later (Fig.17b). The total electron exposure between these two micrographs was quite low (<30 A sec/cm^2), and the changes are as expected for RT vacuum annealing. After taking the micrograph of Fig.17b, the air exposure was conducted, and 20 hrs later Fig.17c was taken. The additional electron irradiation was again only <30 A sec/cm^2. The electron exposure was then deliberately increased by 250 A sec/cm^2 (using 0.8 A/cm^2 current density) to produce Fig. 17d. The progression of both particle spreading and generation of phase contrast features is much increased after the air exposure (compare Fig.17c with b and Fig.17b with a, and compare also with the not air-exposed sample of Fig. 16d). Furthermore, the dependence of the magnitude of this effect on the sample thickness is quite evident, when we compare with the original state immediately following the deposition (Fig.17a), which

clearly shows the substrate steps and areas of equal thickness by contrast variations from step to step. Thin substrate areas show the least effect.

It should be noted that a certain, not negligible effect of electron irradiation damage was noted also for plain MgO substrates without Pd deposit. Under otherwise comparable conditions, Fig.18 shows a {111} MgO area (top) and {100} area (bottom) immediately following e-beam flash heating (a), 240 A sec/cm^2 of 0.2 A/cm^2 irradiation later (b), additional 720 a sec/cm2 later (c), and 720 A sec/cm^2 after an air exposure and 20 hrs of RT-annealing (d) following Fig. 18c. A micrograph (not shown) taken before the 720 A sec/cm^2 irradiation but after the air exposure looked identical to Fig.18c. Fig. 18 demonstrates that the electron irradiation damage effect is strongest in the thicker specimen regions.

DISCUSSION

There are striking differences between the results obtained for MgO and alumina substrates. Under virtually identical experimental conditions, RT-deposits seem to be less thick (in average thickness) on MgO, they are highly epitaxially oriented on MgO and almost completely random on alumina, and their diffraction intensities are unusually broad on MgO. Effects of exposure to gases and laboratory air were noted in both cases, but they were found to be less severe for Pd/alumina. A separate discussion of the results for (i) the nucleation and early growth, (ii) epitaxy and pseudomorphism, and (iii) annealing, gas exposures, and electron- beam enhancement follows.

(1) NUCLEATION AND EARLY GROWTH

The apparent difference in deposit thickness can in part be explained as due to a substantially lowered condensation probability in the case of Pd/MgO. One can estimate the condensation probability from the TEM results. If we assume that the particles have essentially a hemispherical shape and that the condensation probability (Po) on the (heavily Pd-coated) quartz crystal is unity, the condensation probability (P) on the MgO substrate equals the average thickness (M) of actually deposited palladium divided by the thickness (Mo) monitored with the quartz crystal microbalance. Using the mean particle number

density (N) and the mean particle diameter (D) defined earlier in this report, we obtain

$$P = Po \times M/Mo \approx 10^{-14} \frac{\pi}{12} N D^3 Po/Mo \qquad (3)$$

For the case of a nominal 0.3 - 1.8 nm Pd deposit on MgO, such as shown in Fig.4, this equation yields a dependence of the condensation probability on the deposit thickness as shown in Fig. 19, plotted separately for Pd/MgO{100} (solid curve) and Pd/MgO{111} (dash curve). The initial decrease of P with increasing thickness might be due to nucleation at preferred sites. Once all sites have been filled, a further increase in deposit thickness would be expected to justify an increase in the condensation probability, since a more substantial fraction of adatoms impinges on palladium islands where the sticking probability can be expected to be high. The results plotted in Fig.19 are in qualitative agreement with this reasoning, although the difference between the results obtained on the two types of MgO surfaces cannot as readily be understood. One possible explanation might be that the assumption of hemispherical particles is not satisfactory for low deposit thicknesses, i.e., that the Pd particles are particularly flat during the early stage of growth. In fact, AES and UPS studies by Gaebler and coworkers (10) indicate layer growth for Pd deposited at RT onto clean ZnO surfaces. Their results imply, however, layer growth beyond a deposit thickness of

3 nm, which clearly differs from our results for Pd/MgO.

Corresponding calculations of the sticking coefficient for Pd on sapphire yield much higher values of 0.27 for the 0.2 nm nominal deposit case (Fig.3) and 0.47 for 0.6 nm deposit thickness (Fig.1). There seems to be no significant influence of the substrate temperature during deposition on the condensation probability in the temperature range between RT and 500 C, the temperature prevailing during the 0.6 nm deposition experiment.

These findings of a substantially higher condensation probability for the Pd/sapphire system when compared to Pd/MgO, complemented with results reported for Pd/mica (11), where a condensation coefficient of 0.6 was found, indicate that for a substrate /overgrowth system with strong metal support interaction -- which we suppose exists in the case of Pd/MgO as will be discussed below, and to a lesser degree for Pd/mica (11) -- one does not necessarily find a correspondingly high adatom sticking probability.

(2) EPITAXY AND PSEUDOMORPHISM

The results indicate that palladium grows perfectly epitaxially on MgO at temperatures as low as RT, whereas epitaxy on sapphire surfaces requires some 500 C. A comparatively low epitaxial temperature (Te) for Pd was found by various other investigators: Doering et al. (11) found a slight texture for Pd/mica at 200 C and explained this as due to an appreciable degree of metal - support interaction. Christman and Ertl (12) report an optimum temperature for Pd/NaCl of 200 C, with 100 C or 300 C yielding strong fiber textures. Murr and collaborators (13) reached essentially the same conclusion. Kato (14), working under 10^{-5} millibar vacuum conditions, found an increase of Te for Pd/KCl and Pd/KBr to Pd/KI from 80 C to 280 C and suggests a correlation between Te and the ionic radius of the anions in the substrate. Gillet and Renou (15) found good epitaxy for Pd/MoS_2 over a wide range of substrate temperatures (Ts). Takayanagi et al. actually performed Pd/MgO studies under conditions similar to ours, but only at elevated substrate temperatures between 200 and 500 C, and in this regime they found perfect Pd/MgO epitaxy (16). Palmberg and Rhodin (17) obtained {100} epitaxy for Pd/MgO (bulk, uhv-cleaved) for Ts>350 C. The low epitaxial temperature for Pd/MgO -- which may actually be well below RT (no indication of improvement of the degree of epitaxy was noted in our experiments for Ts>RT, and Ts<RT was not attempted) -- compared with the much higher epitaxial

temperature for Pd/sapphire under otherwise very comparable conditions, is another indication of the well-known fact (18) that the geometric registry between overgrowth and substrate (8% for bulk Pd/MgO, less for Pd/sapphire) is not the most important factor in the determination of epitaxy for relatively weakly interacting substrate/overgrowth systems. Surface free energy considerations (17) and electronic interactions between overgrowth and support (19) are much more important factors determining the mode of overgowth (layer vs. three-dimensional deposits) and epitaxy.

One of the more surprising results of this study is that the lattice parameter of Pd on {100} MgO was found expanded by some 3% when compared to the bulk parameter, and the diffraction spots were quite broad (Fig.10). The expansion was highest for the smallest particles. The broadness of the Pd diffraction spots could be due to the small size of the Pd islands. However, our results cannot fully be explained on this basis. The mean particle dimension (D) is related to the diffraction broadening (B) via the Scherrer formula (20)

$$D = K\lambda/(B \cos\Theta_0) \qquad (4)$$

where (K) is a constant factor close to unity, (λ) is the (electron) wave length and (Θ_0) is the Bragg angle. The

broadening (B) is measured in radians. Using the mean particle sizes computed with equation (2), equation (4) would cause the Gaussian spot size distributions shown in part A in Fig.20 for the nominal deposit thicknesses 0.8 - 4.8 nm used in our experiments for Pd/MgO. (The integrated intensity was set proportional to the deposit thickness). Averages of many diffraction patterns such as those shown in Fig.10 give, on the other hand, the diffraction intensity distributions shown in B in Fig.20. It is evident that (i) the actual spot sizes are much broader than would be expected if only natural broadening would be present, and (ii) that the tendency of the broadening direction is toward a decrease of the Pd/MgO lattice misfit, which is about 8% for bulk Pd/MgO; i.e., the tendency is for the Pd lattice parameter to increase with respect to the bulk lattice parameter. This result contrasts with various earlier results, such as for gold on mica obtained in our laboratory, where evaluation of substrate lattice plane re \lution, directions and spacings of moire fringes, and shapes of the particles led to the conclusion that the lattice parameter of the gold deposit was actually contracted (by about 1%, decreasing for increasing particle size) when compared to the bulk parameter of gold. This was in spite of the fact that the substrate lattice parameter was actually larger, i.e., the lattice misfit increased rather than decreased in that case (21,22). In ' earlier work, Mays et al. (23) found similar

results for gold on carbon, and Boswell measured lattice shrinkage of almost 2% in gold particles of some 2 nm in diameter (24). The results were explained in terms of surface stress, which is larger for small particles due to the high surface- to- volume ratio. Palmberg and Rhodin (17) refined this explanation for Pd on mechanically cleaved MgO in terms of enhanced surface valency. More recently, Yokozeki (25) examined the question of lattice shrinkage of small particles for the case of lead. He found a modest decrease of the lattice parameter by 0.3% and argues that, although this result agrees with the phenomenological concept of elastic compression due to surface tension, there may well be another explanation, linear thermal expansion, which would qualitatively agree with his results. Yokozeki further points out that an opposite effect, appreciable lattice expansion, would be plausible for interplanar spacings adjacent to a free surface. This argument dates back to work by Burton and Jura (26) who, using Girifalco and Weizer's (27) Morse potential coefficients for fcc metals, calculated the surface distortion in fcc solids. Their results range from 5.5% expansion for Pb over 6.5% for Ag to 12.5% for Ca {100}, the expansion being lower for {110} and {111} surfaces. Tick and Witt (28) later expanded these calculations, using a

$$\phi_{ij} = \frac{-A}{r_{ij}^{q}} + \frac{B}{r_{ij}^{p}} \qquad (5)$$

type potential, with q=4 and p=7 for fcc-type metals and q=6 and p=12 (Lennard-Jones) for molecular crystals. Their resulting fractional increase in interplanar spacing at the surface was 1 - 4% for metals and as much as 15 - 30% for molecular crystals.

Evidence of lattice expansion of Pd on MgO was also found by Anton et al. in recent in-situ TEM diffraction densitometry measurements (29) following a method developed earlier by two of the present authors (30). Takayanagi et al. (16) presented a micrograph of Pd islands deposited at 300 C on MgO showing moire fringes. They measured a fringe spacing of 2.5 nm and suggest that they are 220 -type moires. Under these conditions, a 2.1% lattice expansion would follow for their Pd islands, which would essentially agree with the present work, but only if one disregards the considerably larger particle size in their work. However, their presentation indicates disagreement with our findings concerning the substrate/ overgrowth directions; if the lattice directions are assumed to be correctly indicated, their moires should be of the 200 rather than 220 type; and 200 -type moires with 2.5 nm spacings would, in turn, indicate the bulk lattice parameter of Pd, i.e., the result that one would expect on contaminated MgO surfaces.

Turkevich et al. (31) report a lattice parameter increase

averaging 1.5% over the bulk parameter for Pd chemically precipitated and presumably supported on carbon. Their conclusion is based on TEM lattice images of the palladium particles upwards of 2 nm in size. However, they make no mention of potentially significant image interpretation difficulties that can be present in TEM lattice images unless the focusing and astigmatism conditions are known and carefully taken into consideration, such as by image simulation calculations (32). On the other hand, Woltersdorf et al. (33) interprete the bending of Al/MgO moire fringes toward the edges of small particles as indicative of lattice contraction being most prominent at particle edges. They likewise do not consider dynamical effects. Turkevich et al. (31) do mention, however, two additional results that are of interest in the present situation. First, in otherwise similar lattice parameter determinations of Pt islands they found no lattice expansion, which might give credence to their results for Pd in spite of the theoretical ambiguities mentioned above. Second, they report that the lattice parameters measured for Pd varied substantially from particle to particle.

When speculating about the reason for the broadening of the Pd diffraction spots in our work, two possibilities are presently being considered:

(i) The individual Pd islands, whose mean diameters we estimated with Equ. (2), are not single crystals but some

sort of multiply twinned particles, each twin being of considerably smaller dimension than the whole particle. Therefore, a broader diffraction peak could be expected. This possibility, which follows the reasoning of Solliard (34) who used the diffraction spot size in 40 kV scanning ED experiments of Au and Pt particles to determine that the Au particles were multiply twinned and the Pt particles single crystals, seems unlikely because the absence of diffraction contrast features usually typical of twinning (Figs.13 and 14), as well as the symmetry in the diffraction patterns (Fig.10) clearly indicate that no or only very few Pd islands were multiply twinned; the rest are single crystals. (ii) The lattice parameter changes within the individual particles due to strains exerted most strongly in the Pd/MgO interface layer and decreasing with increasing distance from the substrate. However, such lattice parameter changes within individual small (nanometer -size) particles have been argued to be improbable for the case of multiply twinned gold crystallites, where a departure from the fcc lattice configuration to a rhombohedral or a bco configuration -- uniform within the entire particle -- was shown to be a more probable means to accomodate the geometric misfit for icosahedral and decahedral particles, respectively (35,36). It may well be that this argument could be extrapolated to small particles in general only uniformly strained particles can exist. However, this argument would not

agree with the earlier mentioned work by Yokozeki (25), Burton and Jura (26), and Tick and Witt (28); but one should note that their argument of non-uniform lattice parameters would then be opposite to the case presented here: they explain expansion in interplanar spacings adjacent to a free (vacuum) surface, whereas we discuss such expansion in the overgrowth at the substrate/ overgrowth interface. Particles of different sizes will be capable to accomodate different, yet uniform strains leading to different, within each particle constant lattice parameters. The observations by Turkevich et al. (31) seem to favor this alternative.

A strong metal support interaction is considered the main driving force for the lattice parameter increases observed in our studies. Pseudomorphism (37) is a well-documented phenomenon in very strongly interacting substrate/ overgrowth systems under truly clean experimental conditions (38). For the case of 2 nm size Pd particles on a relatively strongly interacting substrate like MgO under clean experimental conditions, the accomodation of interfacial misfit by uniform particle strain is probably the dominating mechanism. However, when either the substrate/ overgrowth interaction is decreased (e.g, by contamination, or for different materials) substantially and/or when the particles become even smaller ($\lesssim$1 nm), the particle "capillary forces" take over and minimize the

total surface free energy of the system by particle contraction. This is probably the reason why in recent EXAFS/XRD measurements (39) as well as in most older studies which were more dominated by contamination only decreases of next nearest neighbor distances were found.

(2) ANNEALING, GAS EXPOSURES, AND ELECTRON-BEAM ENHANCEMENT

The results indicate that annealing at room temperature, exposure to gases, and exposure to the electron beam all influence the deposit. Due to the nature of in-situ TEM experiments that are performed sequentially and rely on the electron beam for recording purposes, one cannot positively study the effect of any one of these factors independent of the others. The design of the experiments allowed, however, assessment of that nature at least in part. The following trends can be extracted from our results for Pd/MgO:

(i) The effect of annealing at RT under $1x10^{-8}$ millibar vacuum conditions is some coalescence by cluster mobility (or by fast Ostwald ripening at a time constant of $\leq$1 sec). In earlier experiments in our laboratory we examined in-situ the annealing behavior of silver on graphite (40) and gold on MgO (3, 41). In these experiments we were able to clearly differentiate between ripening, occuring over periods of 100 seconds, and mobility events, occurring within $\ll$0.1 seconds. The actual time resolution in the present experiments being only of the order of 1 second, we believe that it is most likely that the mobility of Pd on MgO is similarly fast than for Au/MgO, i.e., that it also occurs at time constants $\ll$0.1 seconds, and that Ostwald ripening can be excluded as a major factor.

(ii) The particles coalescing during RT vacuum annealing do often not sinter into a new, hemispherically shaped single crystal particle, but they rather form "rafts" of

particles, possibly filling gaps between each other by some short-distance auto-diffusion, leaving the area coverage of the substrate with particles essentially unchanged. This finding indicates that in the case of Pd/MgO the second of the two steps (40) comprising full coalescence, i.e., the sintering to a homogeneous new particle, does not often occur. One possible explanation for this observation might be a strong interaction of the palladium with the substrate, thus making diffusion of Pd atoms away from a position near the substrate surface for incorporation into a newly forming, larger particle less likely.

(iii) The uhv-RT annealing effect is relatively strongest for the smallest particle sizes, i.e., for thin deposits, and decreases with increasing deposit thickness. This obser- vation, most clearly demonstrated with Figs. 16 and 9, is in agreement with most other small-particle mobility observations that have been reported and can essentially be reconciled with the reasonable assumption that the activation energy for mobility of a cluster follows an inverse relation to the cluster/substrate contact area.

(iv) The annealing effect is greatly enhanced upon exposure of the Pd deposited MgO surface to laboratory air or to a low-pressure oxygen environment. Demonstrated with Figs.12 and 13 for a medium and heavy Pd deposit on MgO for the case of air exposure, and with Fig.3 and 15 for an oxygen exposure, it is conceivable that the oxygen available for adsorption at the particle and substrate surfaces

deactivates the strong particle/substrate interaction and thus reduces the activation energy for particle mobility. Once exposed to oxygen or laboratory air, the enhanced annealing effect seems to continue for long periods of time (tens of hours, Fig.13d and 15b), whereas it seems to subside comparatively quickly if no oxygen or air exposure is offered to the as-deposited particles (Figs.8, 16c, 9). The circumstance that the long-term RT-annealed particles look substantially different depending on the annealing conditions -- annealing in laboratory air yields particles with more rounded, seemingly hemispherical cross-sections (Fig.13d), those exposed to laboratory air for only a short duration and then annealed under 10^{-8} millibar total pressure conditions flatten on the substrate (Fig.15b) -- may again be related to the availability of oxygen. Once the oxygen chemisorbed on the particles is used up, such as for oxidation of the palladium or a catalytic activity involving the palladium, further chemi- sorbed oxygen is available in the vacuum-annealing case only on the substrate surface. This may cause palladium atoms to diffuse from the particles to the chemisorbed oxygen on the substrate surface, thus producing the TEM appearance of flattening and spreading of the palladium islands. Spreading under somewhat similar conditions has been found for nickel on mica upon oxygen exposure at 300 C (42). However, these authors attributed the spreading to NiO formation. Air-annealed particles have plenty of oxygen

available at any place and any time, thus rendering any spreading and flattening unnecessary. In fact, the evidence is that under these conditions minimization of the particle surface area to a sperical shape eventually becomes predominant, indicating that the metal-substrate interaction is eventually weakened when enough oxygen is being made available from sources other than the substrate itself, and/or if the specimen is exposed to a contaminating environment.

(v) The annealing effect in air/oxygen exposed samples is enhanced by the imaging electron beam. It is unclear at present, if the apparent sensitivity of MgO to electron irradiation damage (Fig.18) is related to the observed enhancement of the spreading/flattening effect (Fig.17). If radiation damage is manifest in destruction on the Mg-O bonds, it is more easy for oxygen from the substrate to be made available to the palladium, possibly enhancing the diffusion of Pd to the oxygen sites. It is unclear if the Pd actually diffuses into the bulk of the substrate in this process. The electron image appearance in thin substrate areas (Fig.17d, upper right) does suggest a homogeneous "mixture" between what used to be the MgO substrate and Pd particles. If this is correct, it would then follow that e-beam irradiation can be an effective means to disperse palladium. It is, of course, also possible to interprete the disappearance of features clearly attributable to Pd and distinguishable from MgO in Fig. 17d as due to

evaporation/desorption, possibly electron-beam stimulated, of palladium.

CONCLUSIONS

Palladium was deposited inside a custom TEM specimen chamber onto clean MgO {100} and {111} and α-alumina surfaces prepared by electron-beam flash-heating. TEM examination of deposits of 0.3 - 1.8 nm nominal thickness yielded results that are consistent with a strong metal - support interaction (SMSI) for Pd/MgO and a weak interaction for the Pd/alumina system. These results include: (i) perfect epitaxy for Pd/MgO already for room-temperature (RT) deposits, and almost completely random orientation of Pd/alumina under the same conditions; (ii) expansion of the Pd lattice by some 2-4%, the largest amounts of expansion being registered for the smallest particles, whereas the expansion measured for Pd/ α-alumina was $\leq$1%; (iii) a spreading of the Pd islands on the MgO substrate upon long-term (tens of hours) high- vacuum annealing at RT after exposure to laboratory air or oxygen; (iv) strong coalescence with subsequent minimization of the surface area of the coalesced particles during long-term (tens of hours) RT exposure to laboratory air; and (v) an increased rate of spreading -- and possibly atomic diffusion into the MgO substrate -- of Pd upon intensive irradiation with the electron beam at rates that were determined to cause significant radiation damage in the bare MgO substrate. Mobilities of particles during annealing of Pd/MgO were observed but occurred less frequently than for Pd/alumina.

The additional result that the sticking probability for RT deposits of Pd on clean MgO is low (<0.1) and about 5 times lower than on clean α-alumina seems inconsistent with the SMSI concept for Pd/MgO..

The experiments clearly indicate that one should exercise caution in the interpretation of ex-situ TEM results obtained from metal deposits that have been exposed to laboratory air during the TEM specimen preparation process. Substantial changes in particle habit and crystal structure, as well as size, area coverage of the substrate, and number density may occur. Changes may even be experienced due to exposure of only a few tens of Langmuirs of gases such as oxygen or air, or even due to mere RT- annealing. These findings underline the importance of in-situ TEM observations when characterizing particulate deposits of catalytically active materials.

REFERENCES

(1) H. Poppa and K. Heinemann, Optik 56, 183, 1980.

(2) G. HonJo, S. Shinozaki, and H. Sato, Appl. Phys. Lett., 9, 23,1966.

(3) J.J. Metois, K. Heinemann, and H. Poppa, Thin Solid Films, 41, 197, 1977.

(4) M.H. Francombe, A.J. Noreika, and S.A. Zeitman, Sect. 6, Final Technical Report, Contract AF 33 (615-3814), BPSN-No. 6-684150-415002, 1960.

(5) K. Heinemann, R. Anton, and H. Poppa, Proceed. 39th EMSA Meeting, Claitor's Publ. Div., 1982, p. 158.

(6) K. Heinemann and T. Osaka, J. Crystal Growth, in print.

(7) K. Heinemann, H.K. Kim, and H. Poppa, J. Vac. Sci. Technol. 16, 622, 1979.

(8) K. Heinemann and H. Poppa, Proceed. 10th Int. Congr. EM, Hamburg, 1982, Vol.2, p. 497.

(9) K. Heinemann and H. Poppa, Appl. Phys. Lett. 20, 122, 1972.

(10) W. Gaebler, K. Jacobi, and W. Ranke, Surf. Sci., 75, 355, 1978.

(11) D.L. Doering, H. Poppa, and J.T. Dickinson, J. Catalysis, 73, 104, 1982.

(12) K. Christmann and G. Ertl, Thin Solid Films, 28, 3, 1975.

(13) L.E. Murr, Thin Solid Films, 7, 101, 1971.

(14) T. Kato, Jap. J. Appl. Phys., 7, 1162, 1968.

(15) M. Gillet and A. Renou, Thin Solid Films, 52, 23, 1978.

(16) K. Takayanagi, K. Yagi, and G. HonJo, Thin Solid Films, 48, 137, 1978.

(17) P.W. Palmberg and T.N. Rhodin, J. Chem. Phys., 49, 134, 1968.

(18) E. Bauer and H. Poppa, Thin Solid Films, 12, 167, 1972.

(19) Yu. Ryndin, R.F. Hicks, and A.T. Bell, J. Catalysis,

70, 287, 1981.

(20) P. Scherrer, Goettinger Nachrichten, 2, 98, 1918.

(21) H. Poppa, K. Heinemann, and A.Grant Elliot, J. Vac. Sci. Technol. 8, 471, 1971.

(22) K. Heinemann and H. Poppa, unpublished results.

(23) C.W. Mays, J.S. Vermaak, and D. Kuhlmann-Wilsdorf, Surf. Sci., 12, 134, 1968.

(24) F.W.C. Boswell, Proceed. Phys. Soc., A64, 465, 1951.

(25) A. Yokozeki, J. Chem. Phys., 68, 3766, 1978.

(26) J.J. Burton and G. Jura, J. Phys. Chem., 71, 1937, 1967.

(27) L.A. Girifalco and V.G. Weizer, Phys. Rev., 114, 687, 1959.

(28) P.A. Tick and A.F. Witt, Surf. Sci., 26, 165, 1971.

(29) R. Anton and H. Poppa, Proceed. 10th Int. Congr. EM, Hamburg, 1982, Vol.2, p.509 and p.511.

(30) K. Heinemann and H. Poppa, Proceed. 9th Int. Congr. EM, Toronto, 1978, 160.

(31) J. Turkevich, L.L. Ban, and J.H. Wall, in "Perspectives in Catalysis in Commemoration of Jons Jacob Berzelius," Oct.1979, R. Larsson, editor; University of Lund, Sweden, p.59.

(32) D.J.H. Cockayne and M. Wilkens, 7th Australian Conf. on EM and Cell Biology, Canberra, 1982, and private communication.

(33) J. Woltersdorf, A.S. Nepijko, and E. Pippel, Surf. Sci., 106, 64, 1981.

(34) C. Solliard, Surf. Sci., 106, 58, 1981.

(35) K. Heinemann, M.J. Yacaman, C.Y. Yang, and H. Poppa, J. Crystal Growth, 47, 177, 1979.

(36) M.J. Yacaman, K. Heinemann, C.Y. Yang, and H. Poppa, J. Crystal Growth, 47, 187, 1979.

(37) J.H. van der Merwe, Thin Solid Films, 74, 129, 1980; also in: R. Vanselow (ed.), Chemistry and Physics of Solid Surfaces, Vol.2, Chem. Rubber Co., Boca Raton, 1979.

(38) E. Bauer, "Epitaxy of Metals on Metals," Int. Conf. on Surfaces and Thin Films, Appl. Surf. Sci., to be published.

(39) P. Gallezot and G. Bergeret, J. Catalysis, 72, 294, 1981.

(40) K. Heinemann and H. Poppa, Thin Solid Films, 33, 237, 1976.

(41) J.J. Metois, K. Heinemann, and H. Poppa, Phil. Mag., 35, 1413, 1977.

(42) D.L. Doering, J.T. Dickinson, and H. Poppa, J. Catalysis, 73, 91, 1982.

FIGURE CAPTIONS

Fig.1. Typical 0.6 nm RT-deposit of Pd on sapphire.

Fig.2. 0.6 nm RT-deposit of Pd on sapphire after annealing at 600 C. Indicated reflections are 111 Pd and $1\bar{2}10$ α-Al_2O_3.

Fig.3. 0.2 nm deposit of Pd/sapphire; (a) after RT-deposition (very small particles, randomly oriented), (b) after 3 min anneal at 500 C and 2×10^{-8} millibar total pressure (particles coalesced to 3.3 nm mean size, epitaxially oriented); (c) after 10 min oxygen exposure at 200 C and 10^{-6} millibar (much additional coalescence); (d) after additional hydrogen exposure at 200 C (no apparent additional changes). 220 reflections of Pd indicated as reference. Dots are alumina, arcs are Pd reflections.

Fig.4. Typical RT-deposit of Pd on {100} MgO; nominal thickness 0.3 nm (a), 0.6 nm (b), 1.2 nm (c), and 1.8 nm (d).

Fig.5. Particle number density (N) vs. nominal deposit thickness for Pd/MgO {100} and {111}.

Fig.6. Particle area coverage (θ) vs. nominal deposit thickness for Pd/MgO {100} and {111}.

Fig.7. Mean particle diameter (D, computed from equ.(2)) vs. nominal deposit thickness for Pd/MgO {100} and {111}.

Fig.8. Deposition - annealing sequence of Pd, RT-deposited at 0.3 nm nominal thickness onto {100} MgO. (a) substrate after e-beam "cleavage" before deposition; (b) shortly after deposition; (c) 21 hrs after deposition; (circle indicates example of particle coalescence, square of mobility).

Fig.9. 1.2 nm (nominal) deposit of Pd on MgO; left: 28 min after end of deposition; right: after 24 hour RT-anneal at 1×10^{-8} millibar. Very few changes have occurred due to large size of particles.

Fig.10. Typical selected-area diffraction pattern of Pd/MgO {100} of 1.2 nm (left) and 1.8 nm (right) nominal thickness.

Fig.11. Pd/MgO (0.3 nm nominal thickness) 7 min after deposition (a); and 2.5 min (b), 36 min (c), and 200 min (d) after exposure to oxygen for 3 min at

2×10^{-6} millibar. Circles indicate examples of coalescence, triangle of shape change.

Fig.12. Pd/MgO {111} deposit (0.9 nm nominal thickness) before (left) and 5 hrs after 10 min exposure to laboratory air (right), exhibiting much coalescence and particle mobility, often ending at steps.

Fig.13. Pd/MgO {100} (1.8 nm nominal thickness) shortly after deposition (a); after 10 min exposure to laboratory air (b); after 30 additional minutes of exposure to air (transfer to other microscope, (c)); and after 120 hrs exposure to laboratory air (d). Circle depicts randomly selected area for easier comparison.

Fig.14. Long-term air-exposed Pd/MgO{100}. Left: BF-image; center: focussed Pd 200 SZDF image; right: double exposure of focussed and defocussed Pd 200 SZDF images.

Fig.15. Pd/MgO ({111} area in lower half, {100}area in upper half; 0.3 nm nominal deposit thickness); left: before exposure, right: 100 hrs after anneal in oxygen for 3 min at 2×10^{-6} millibar, exhibiting particle flattening.

Fig.16. Pd/MgO {100} (0.6 nm nominal thickness); (a) immediately after end of deposition; (b) 200 min later; (c) and (d) 15 hrs later; (d) has obtained 150 A sec/cm2 additional electron irradiation, causing radiation damage-induced particle flattening.

Fig.17. Pd/MgO {111} (0.3 nm nominal thickness) immediately after deposition (a); 100 hrs later (b); after additional 20 hrs vacuum annealing following a 10-min air exposure (c); and after additional 250 A sec/cm2 electron irradiation (d).

Fig.18. MgO substrate immediately following e-beam "cleavage" (a); after 240 A sec/cm2 (b) and after additional 720 A sec/cm2 (c) electron irradiation; and after air exposure and additional electron irradiation (d).

Fig.19. Condensation probability (P) for Pd/MgO {100} and {111}, computed with equation (3).

Fig.20. Diffraction intensity distributions for various mean particles sizes, computed with equ.(4) (A); and measured for Pd/MgO (B).

Fig.1

ORIGINAL PAGE IS
OF POOR QUALITY

ORIGINAL PAGE IS
OF POOR QUALITY

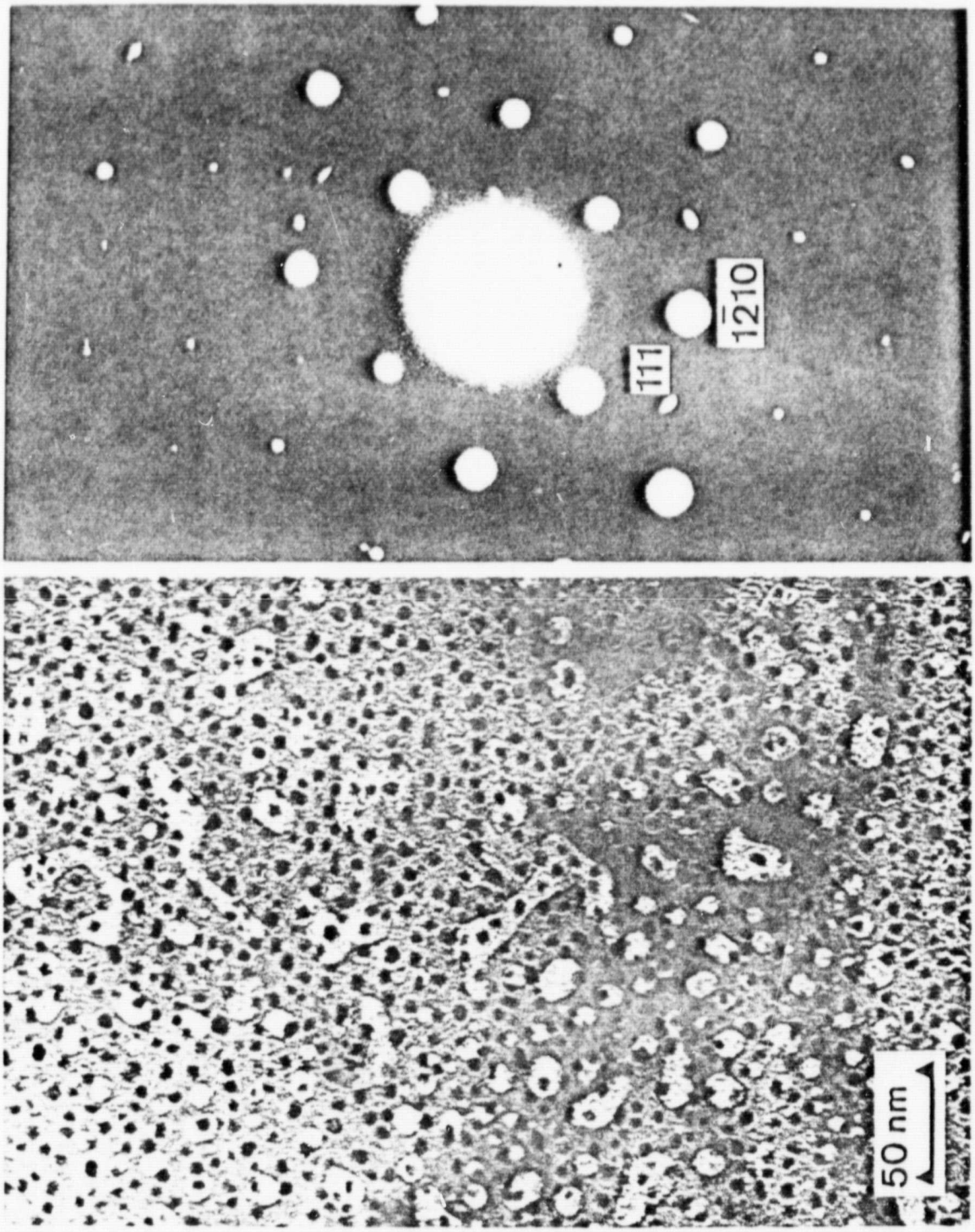

Fig.2

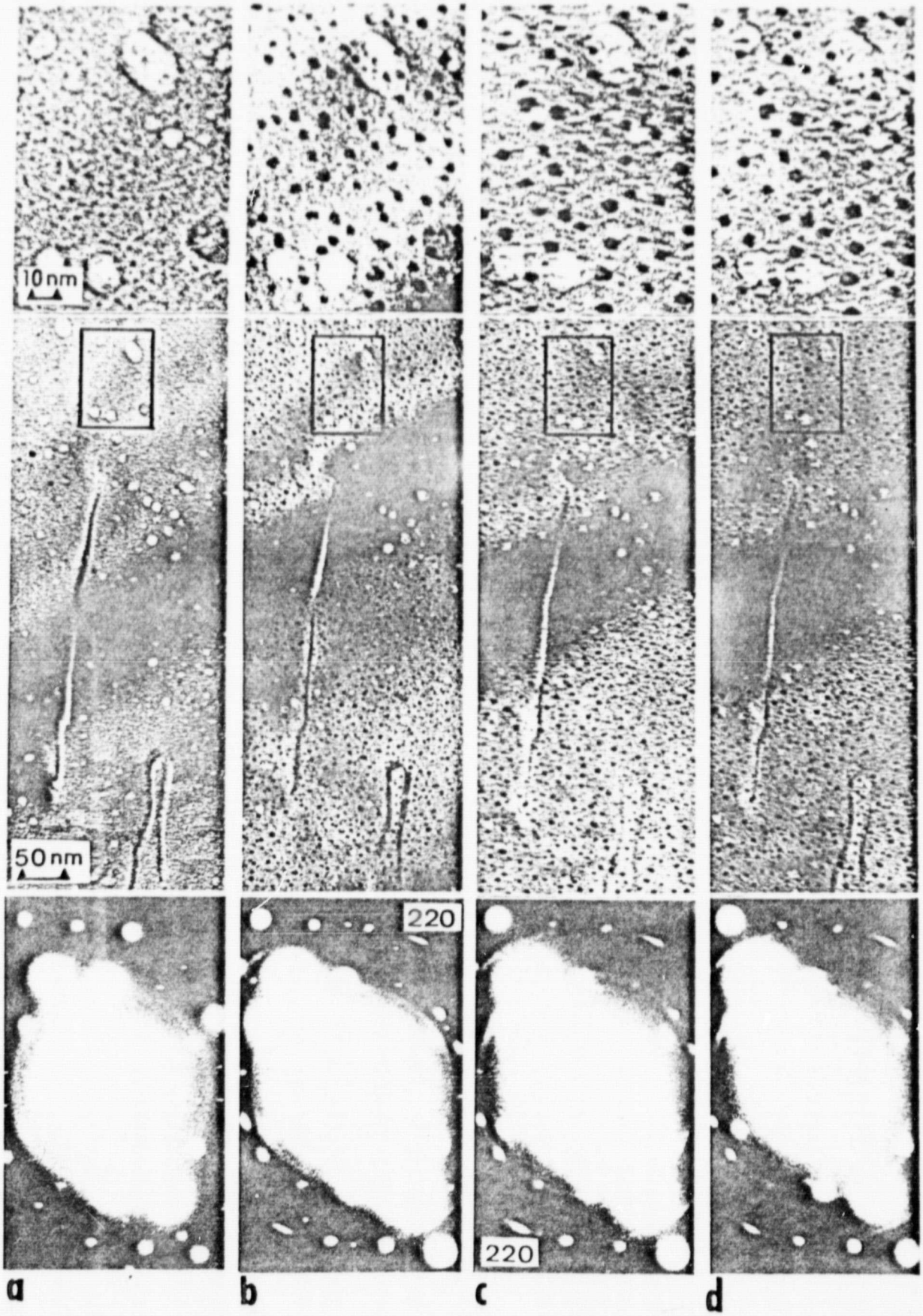

Fig.3

ORIGINAL PAGE IS
OF POOR QUALITY

Fig.4

ORIGINAL PAGE IS
OF POOR QUALITY

ORIGINAL PAGE IS
OF POOR QUALITY

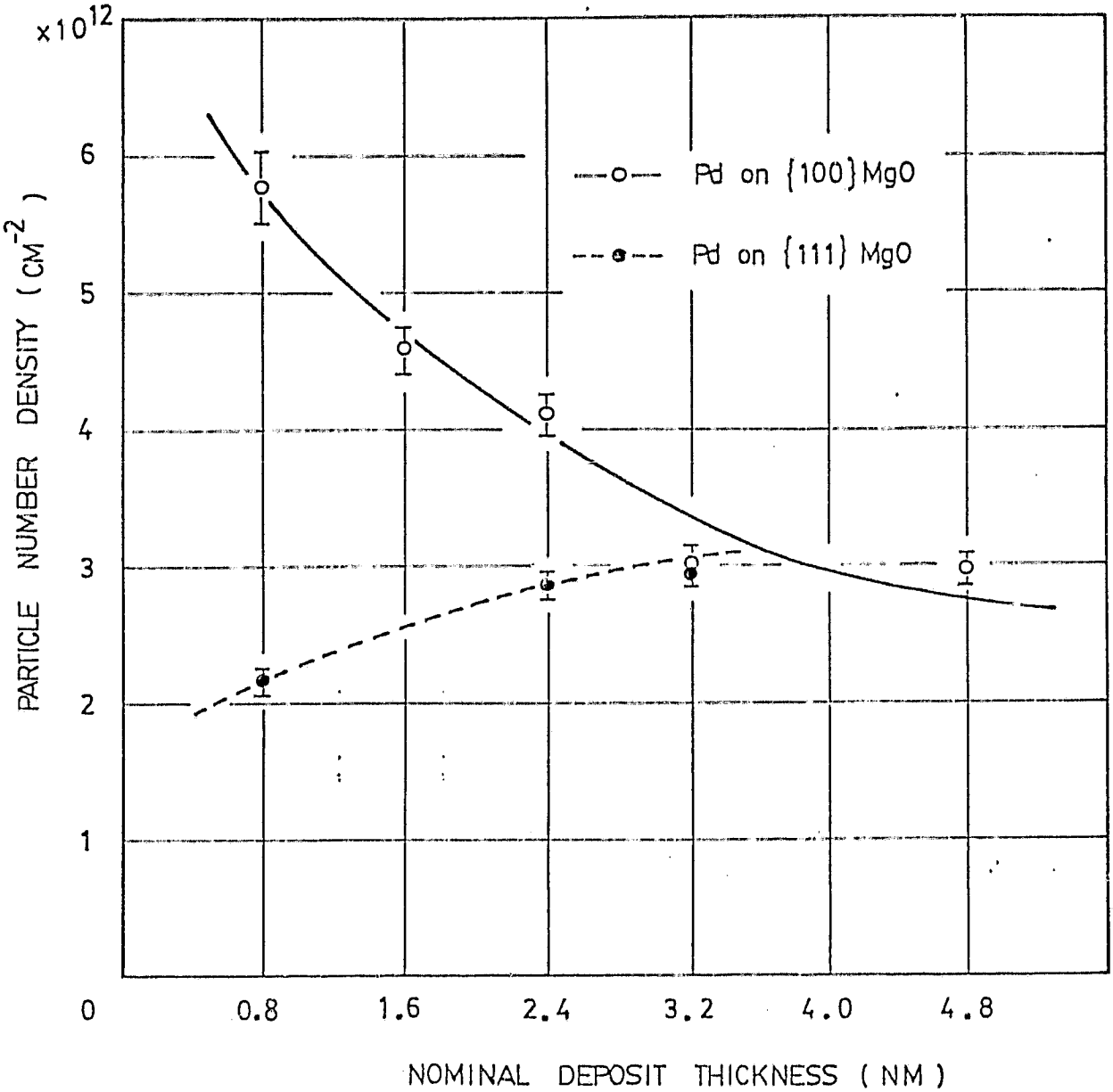

ORIGINAL PAGE IS
OF POOR QUALITY

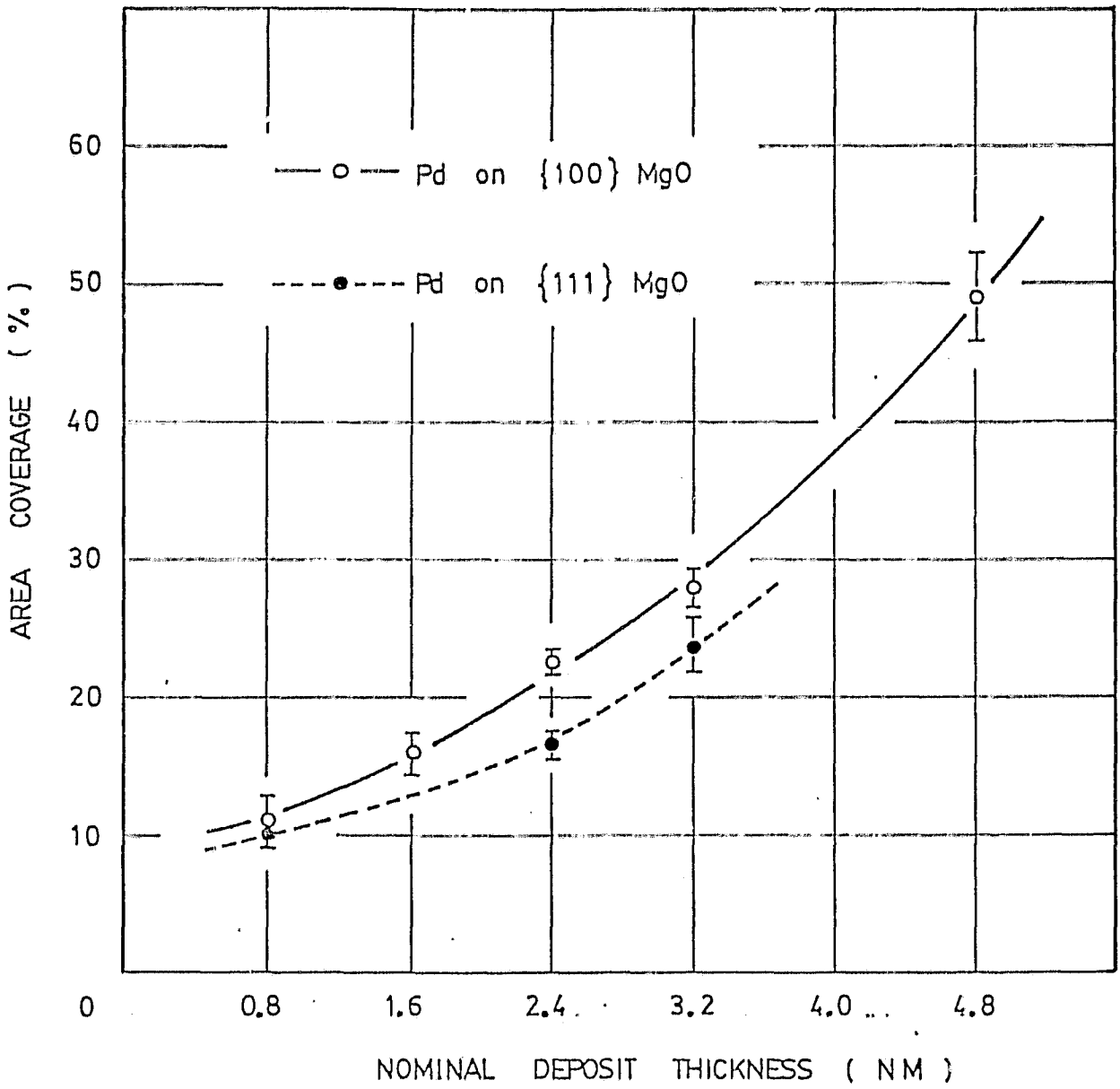

ORIGINAL PAGE IS
OF POOR QUALITY

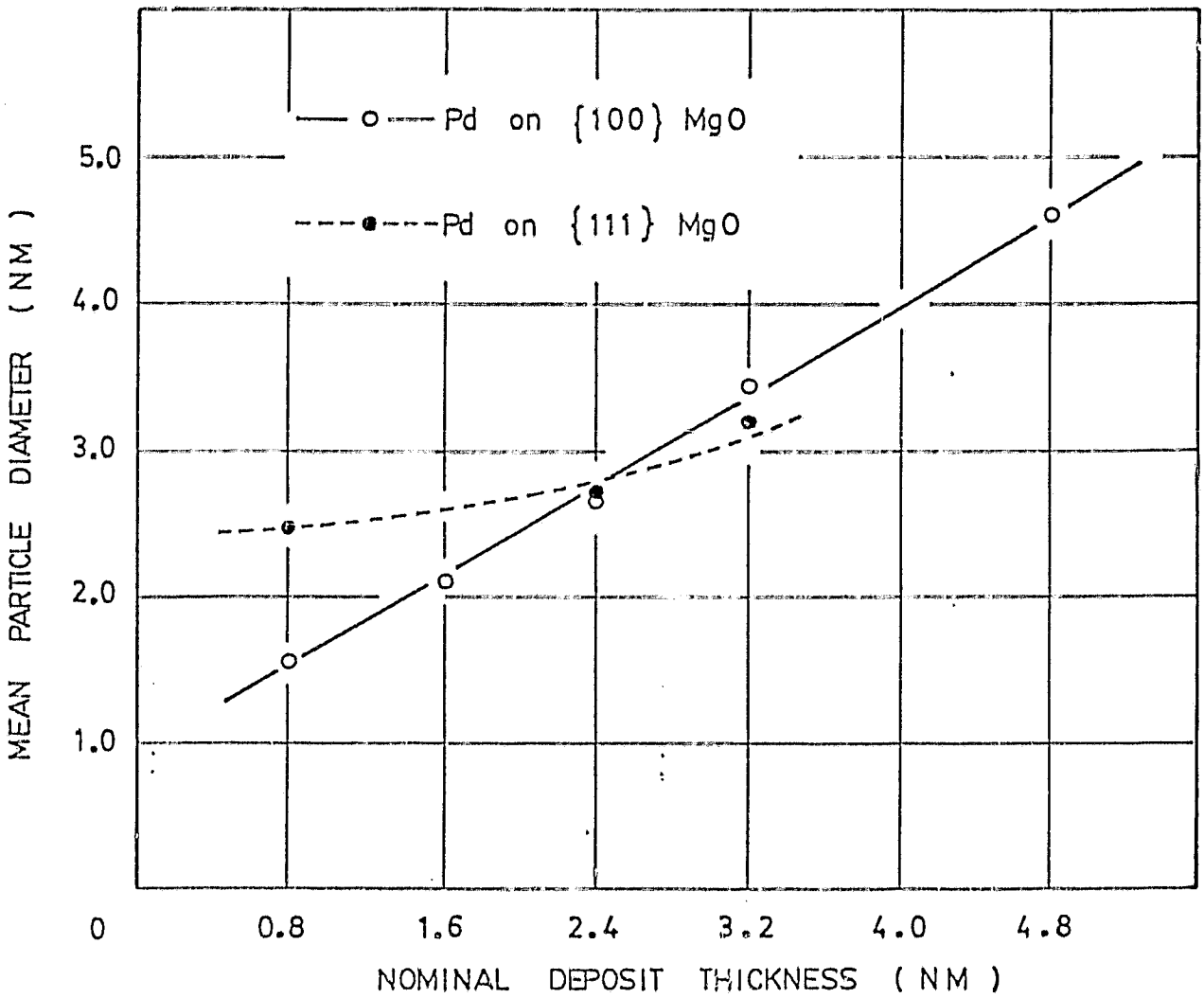

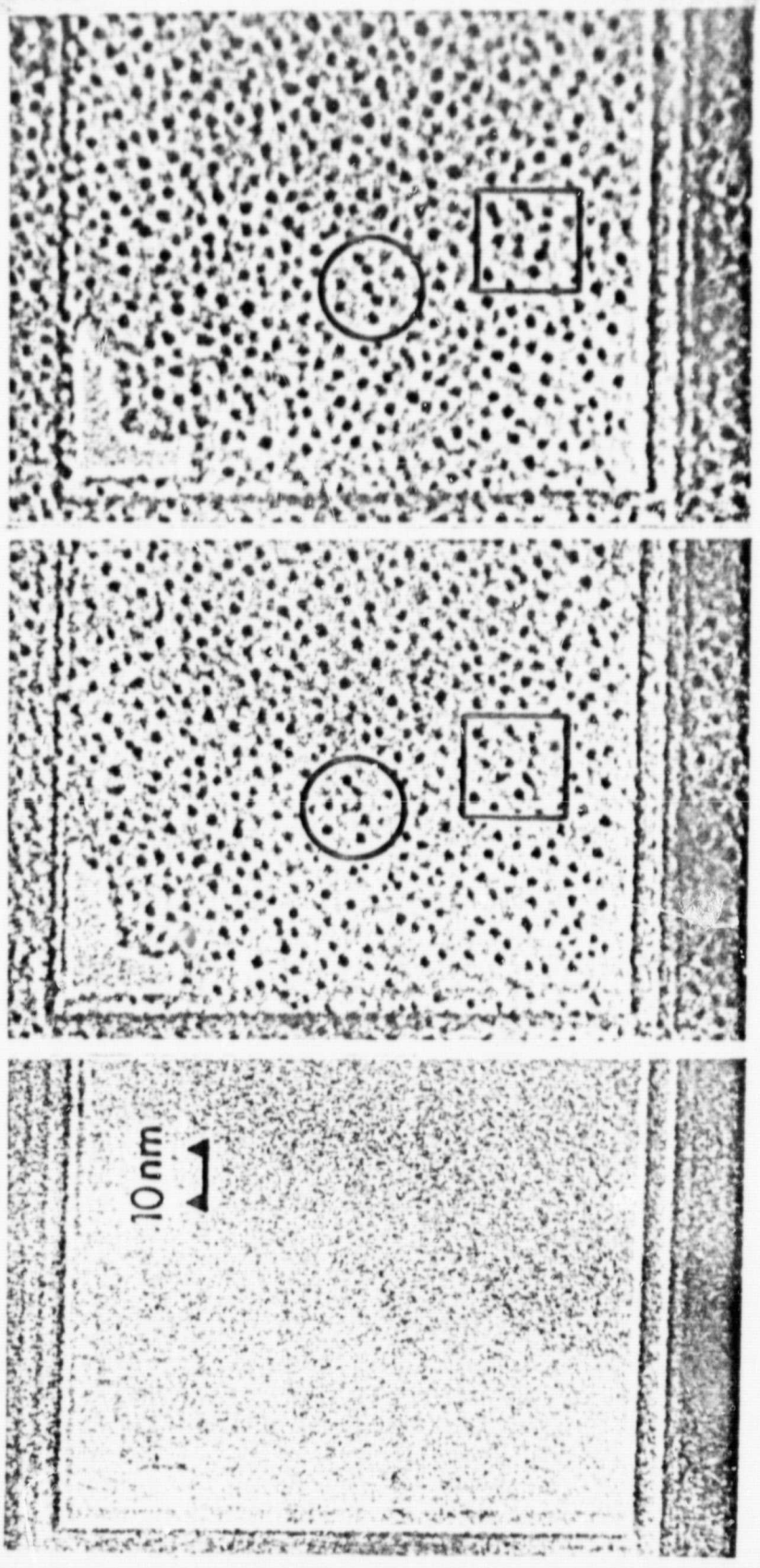

ORIGINAL PAGE IS
OF POOR QUALITY

Fig.8

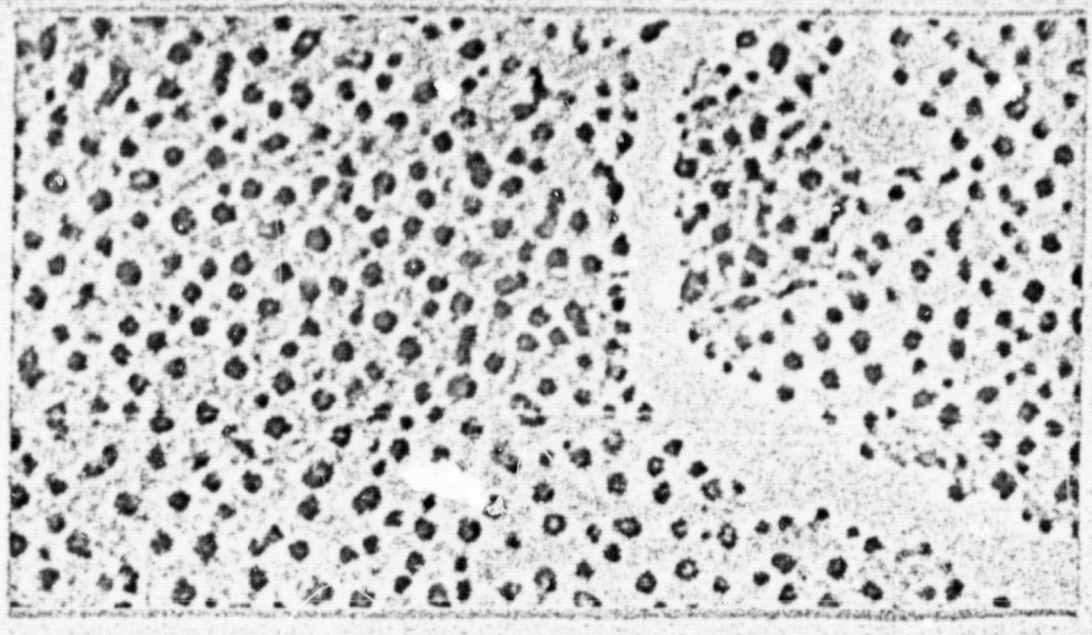

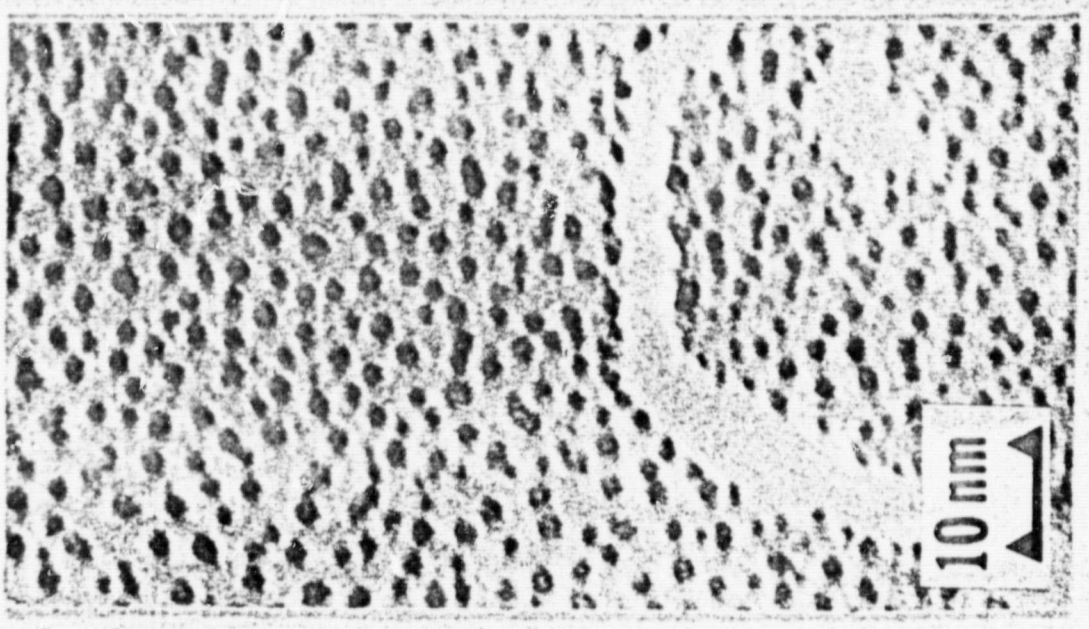

Fig.9

ORIGINAL PAGE IS
OF POOR QUALITY

ORIGINAL PAGE IS
OF POOR QUALITY

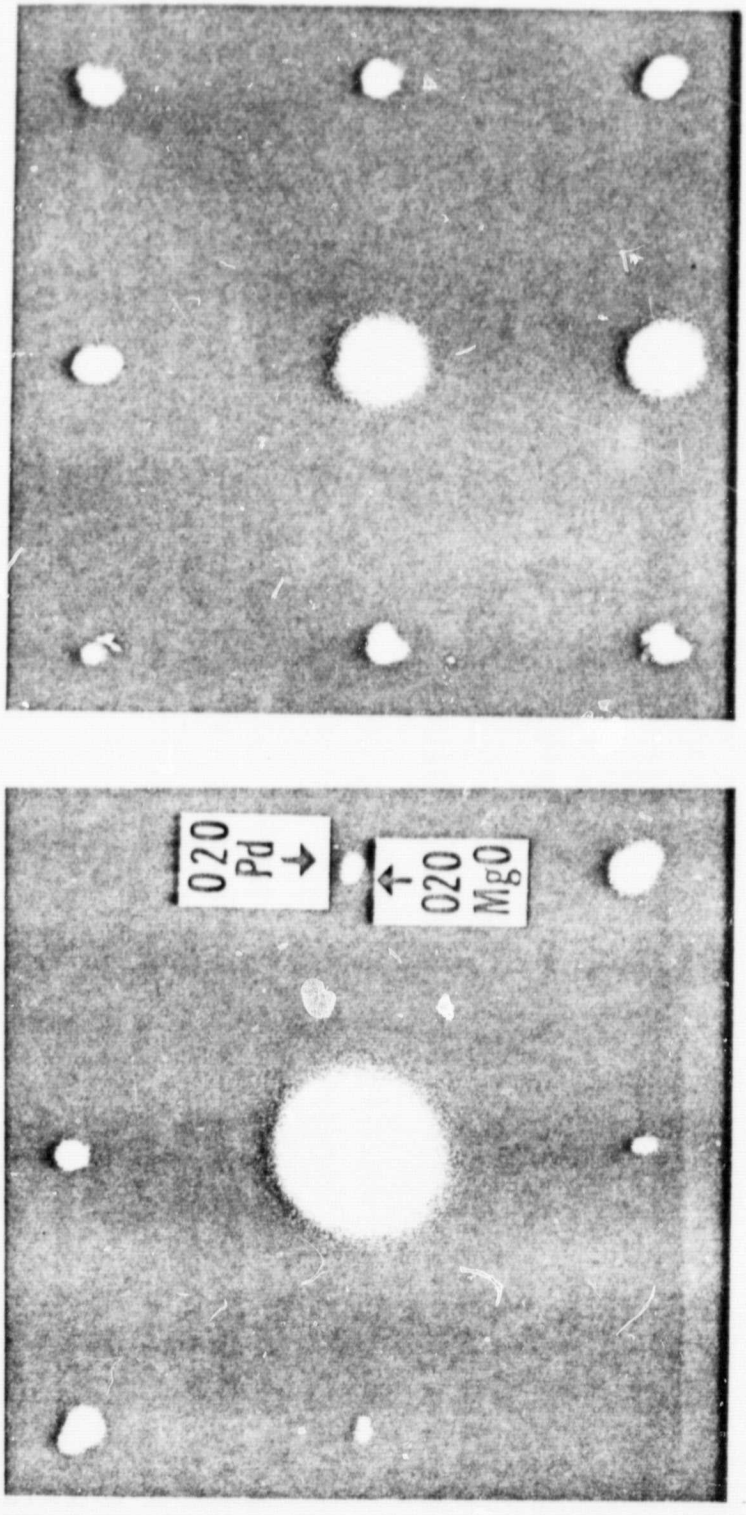

Fig.10

Fig.11

ORIGINAL PAGE IS
OF POOR QUALITY

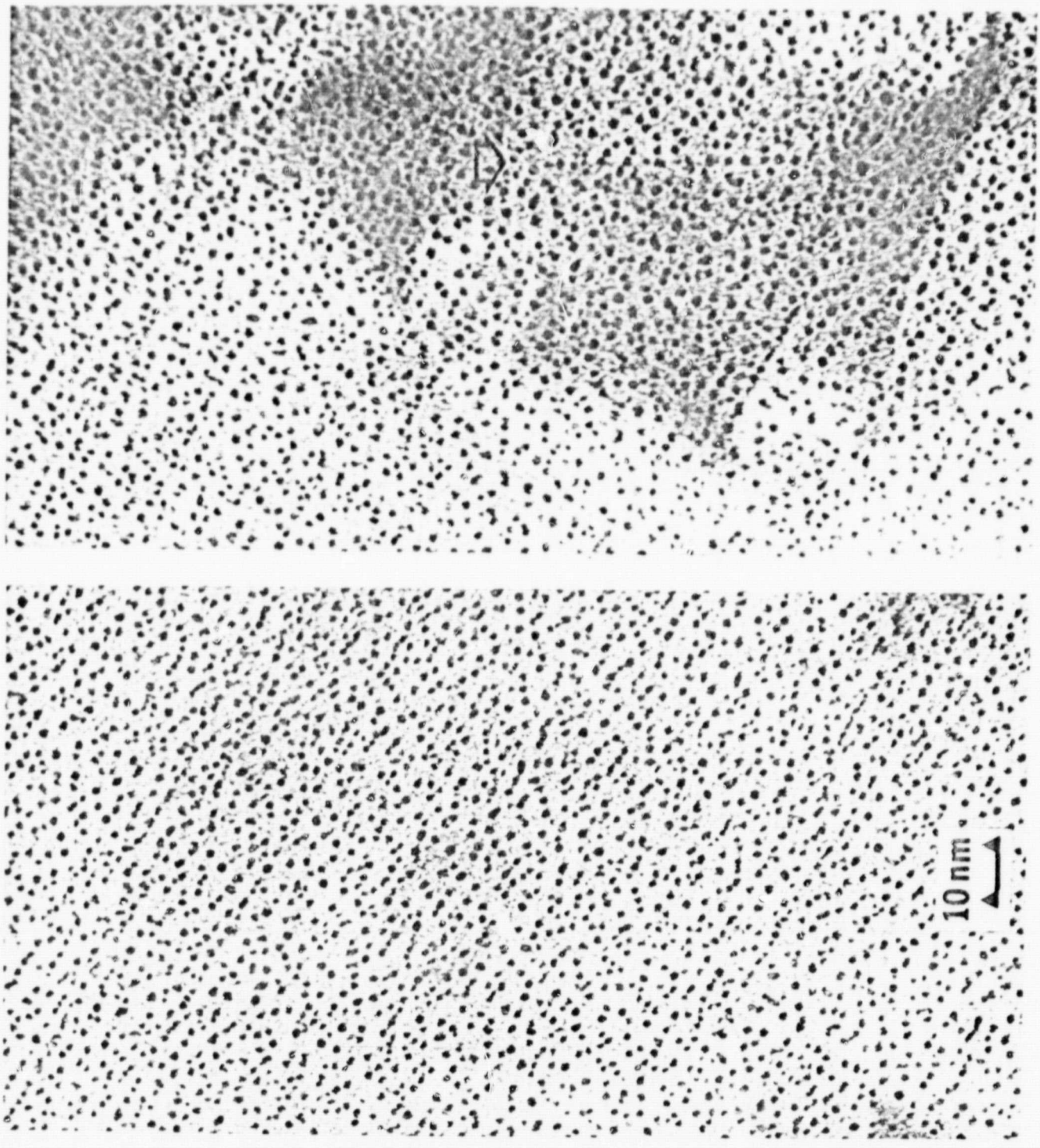

Fig.12

ORIGINAL PAGE IS
OF POOR QUALITY

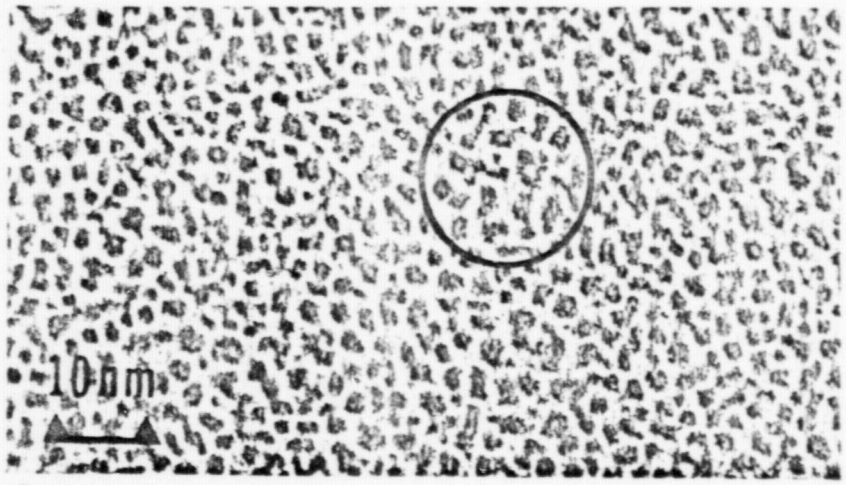

a

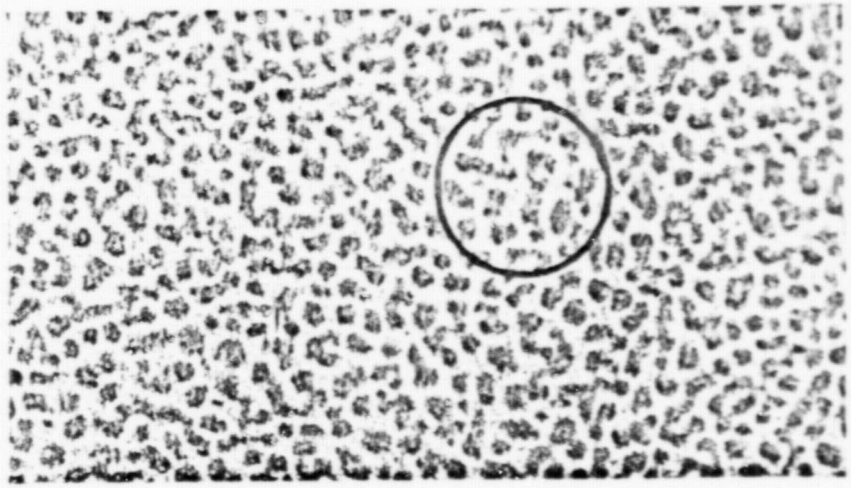

b

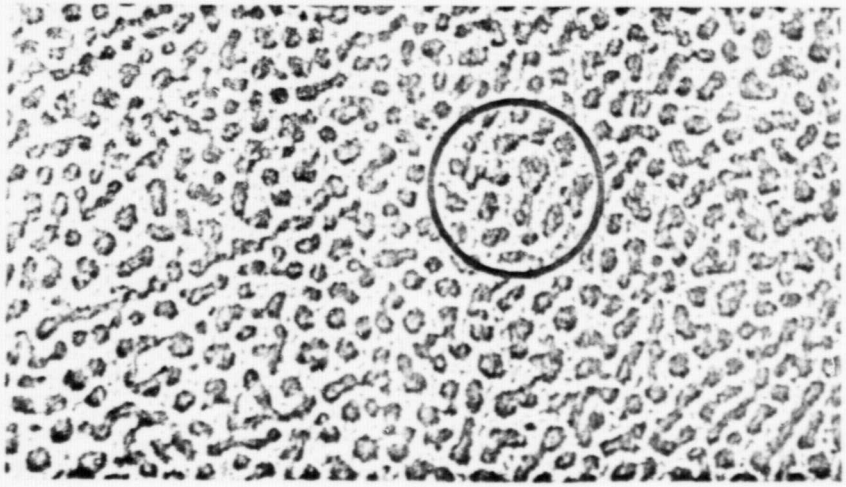

c

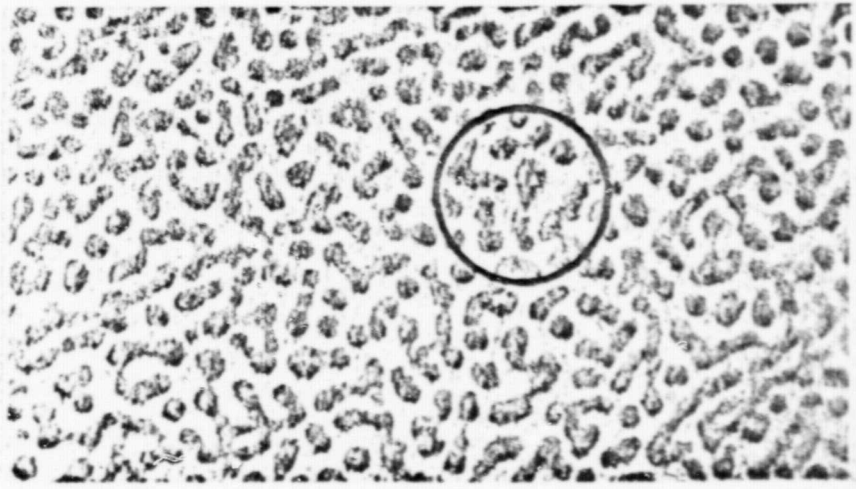

d

Fig.13

ORIGINAL PAGE IS
OF POOR QUALITY

ORIGINAL PAGE IS
OF POOR QUALITY

Fig.14

ORIGINAL PAGE IS
OF POOR QUALITY

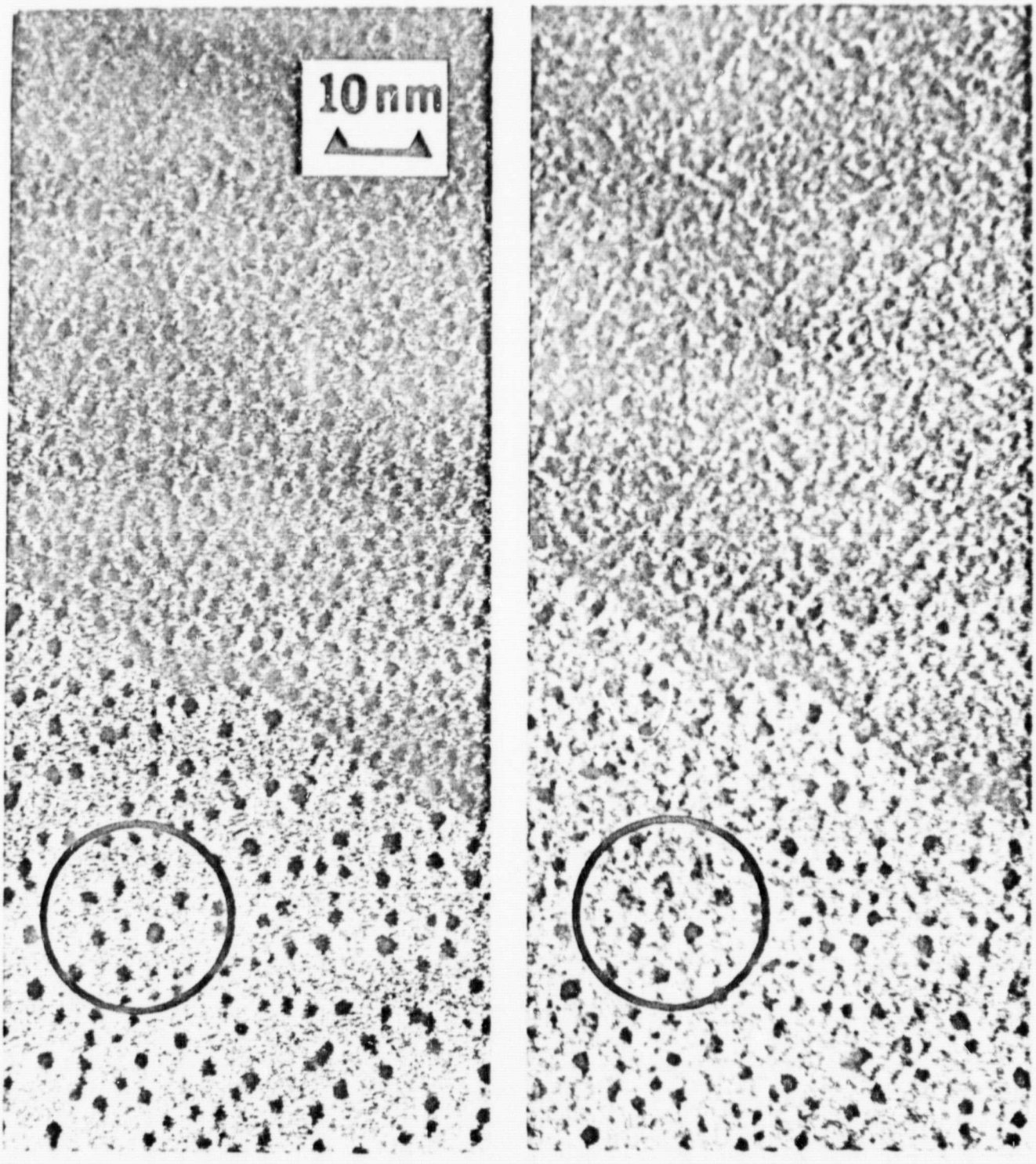

Fig.15

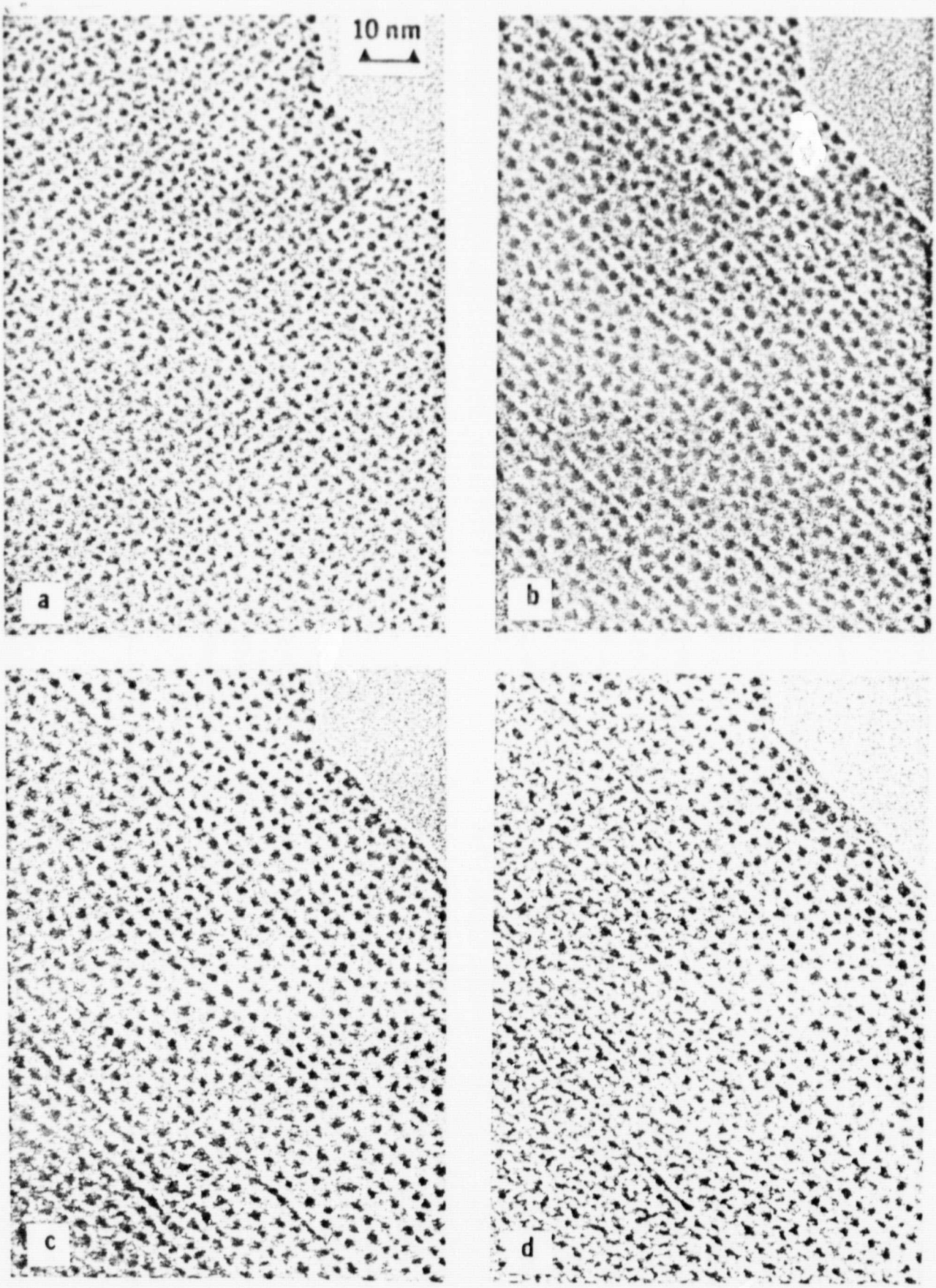

Fig.16

ORIGINAL PAGE IS
OF POOR QUALITY

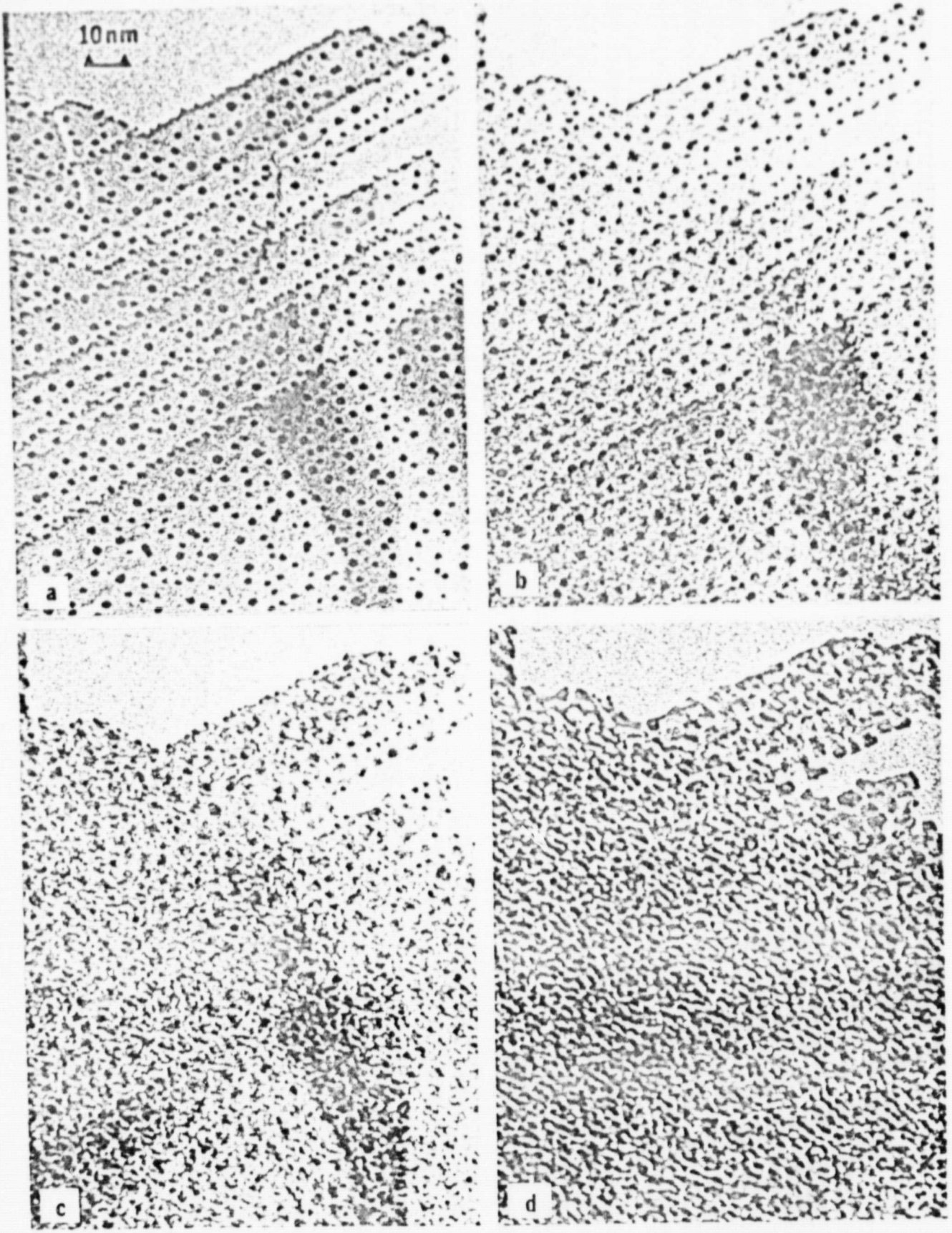

Fig.17

ORIGINAL PAGE IS
OF POOR QUALITY

ORIGINAL PAGE IS
OF POOR QUALITY

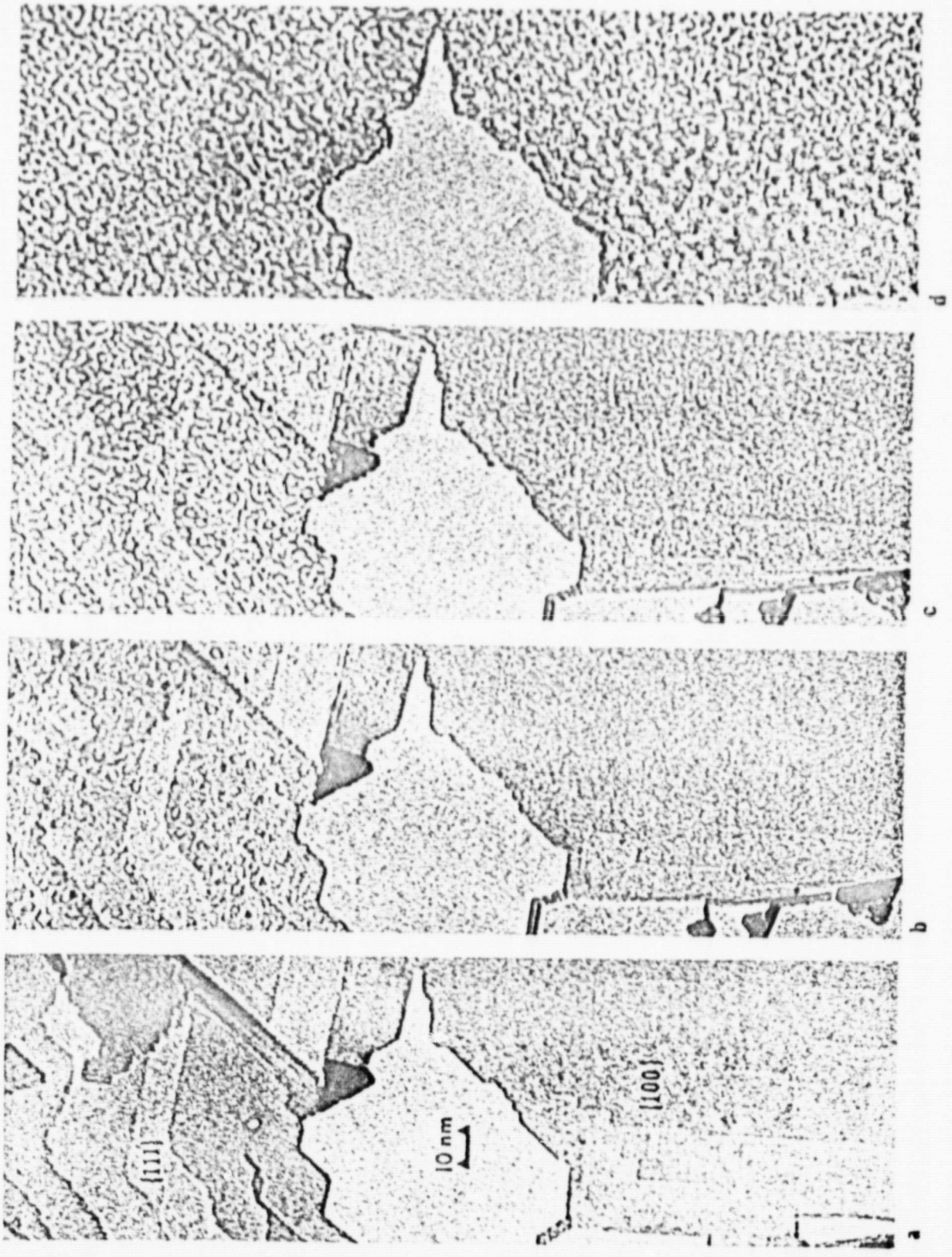

Fig.18

ORIGINAL PAGE IS
OF POOR QUALITY

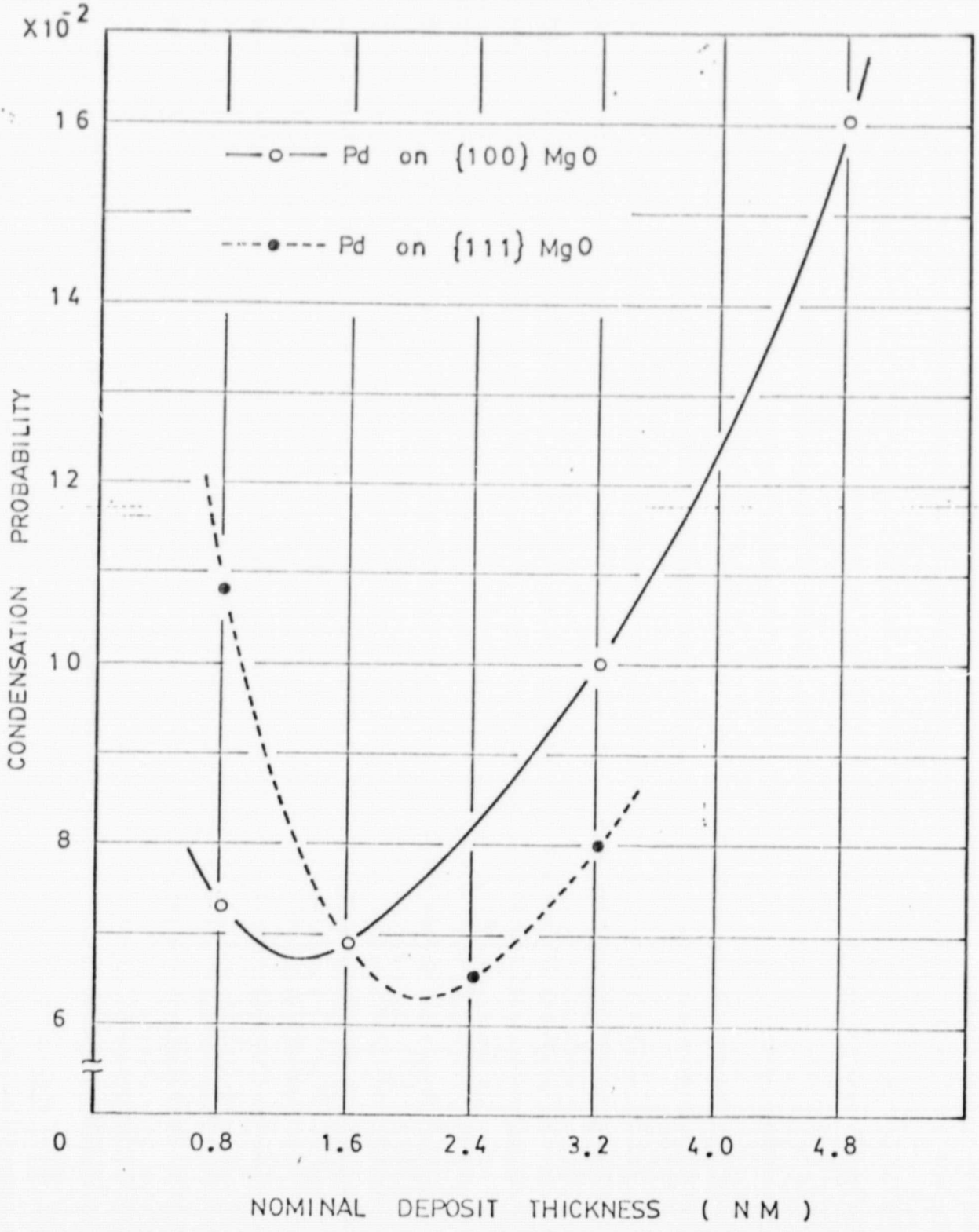

ORIGINAL PAGE IS
OF POOR QUALITY

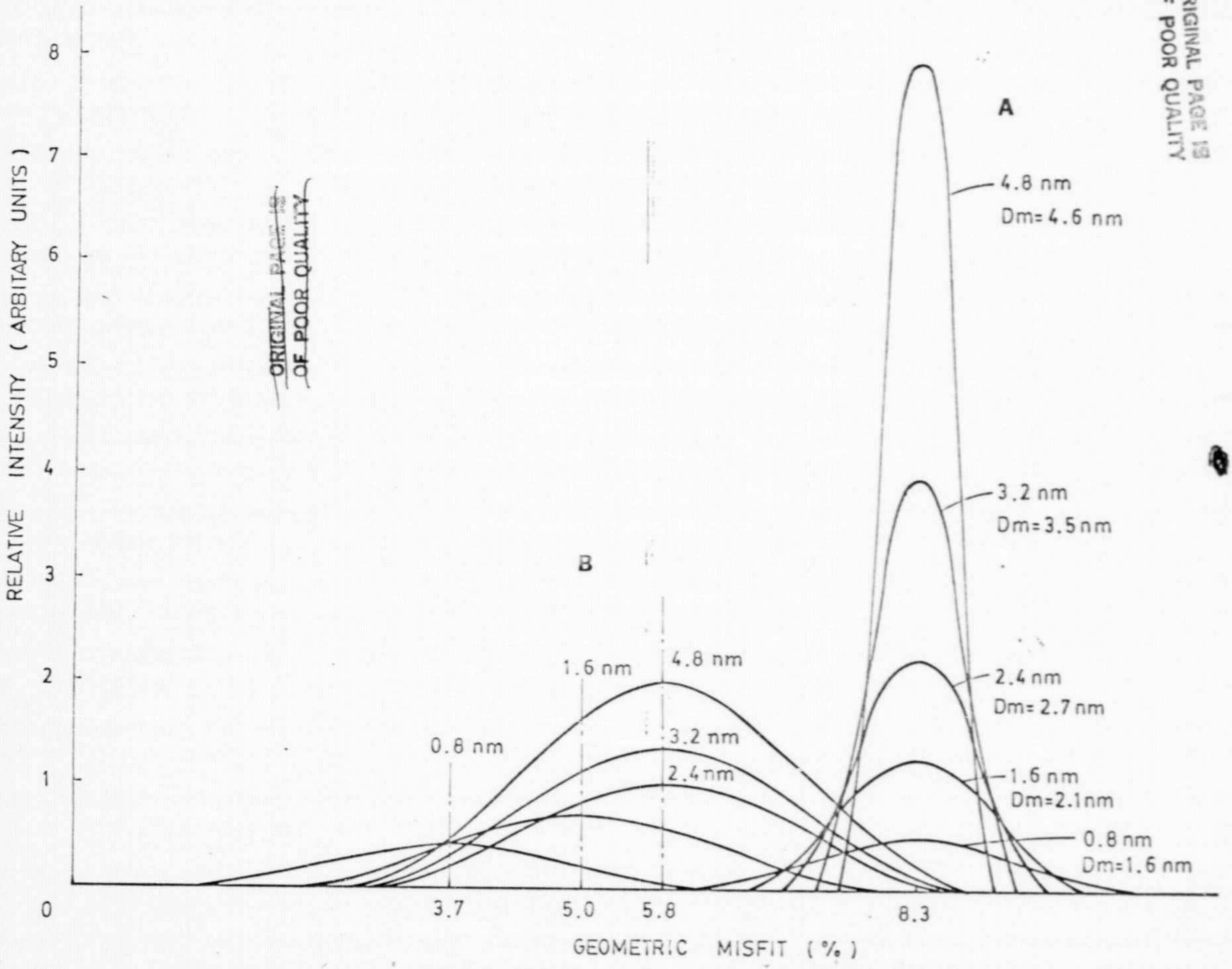

ORIGINAL PAGE IS
OF POOR QUALITY